JCI The Journal of Clinical Investigation

FGF23 induces left ventricular hypertrophy

Christian Faul, … , Martin G. Keane, Myles Wolf

J Clin Invest. 2011;121(11):4393-4408. https://doi.org/10.1172/JCI46122.

Research Article **Nephrology**

Chronic kidney disease (CKD) is a public health epidemic that increases risk of death due to cardiovascular disease. Left ventricular hypertrophy (LVH) is an important mechanism of cardiovascular disease in individuals with CKD. Elevated levels of FGF23 have been linked to greater risks of LVH and mortality in patients with CKD, but whether these risks represent causal effects of FGF23 is unknown. Here, we report that elevated FGF23 levels are independently associated with LVH in a large, racially diverse CKD cohort. FGF23 caused pathological hypertrophy of isolated rat cardiomyocytes via FGF receptor–dependent activation of the calcineurin-NFAT signaling pathway, but this effect was independent of klotho, the coreceptor for FGF23 in the kidney and parathyroid glands. Intramyocardial or intravenous injection of FGF23 in wild-type mice resulted in LVH, and klotho-deficient mice demonstrated elevated FGF23 levels and LVH. In an established animal model of CKD, treatment with an FGF–receptor blocker attenuated LVH, although no change in blood pressure was observed. These results unveil a klotho-independent, causal role for FGF23 in the pathogenesis of LVH and suggest that chronically elevated FGF23 levels contribute directly to high rates of LVH and mortality in individuals with CKD.

FGF23 induces left ventricular hypertrophy

Christian Faul,[1,2] Ansel P. Amaral,[1,2] Behzad Oskouei,[3] Ming-Chang Hu,[4,5,6] Alexis Sloan,[1,2] Tamara Isakova,[1] Orlando M. Gutiérrez,[7] Robier Aguillon-Prada,[1] Joy Lincoln,[8] Joshua M. Hare,[3] Peter Mundel,[9] Azorides Morales,[10] Julia Scialla,[1] Michael Fischer,[11,12] Elsayed Z. Soliman,[13] Jing Chen,[14] Alan S. Go,[15] Sylvia E. Rosas,[16] Lisa Nessel,[17] Raymond R. Townsend,[16] Harold I. Feldman,[16,17] Martin St. John Sutton,[18] Akinlolu Ojo,[19] Crystal Gadegbeku,[20] Giovana Seno Di Marco,[21] Stefan Reuter,[21] Dominik Kentrup,[21] Klaus Tiemann,[22] Marcus Brand,[21] Joseph A. Hill,[4,23] Orson W. Moe,[4,6,24] Makoto Kuro-o,[6,25] John W. Kusek,[26] Martin G. Keane,[18] and Myles Wolf[1]

[1]Division of Nephrology and Hypertension, Department of Medicine, [2]Department of Cell Biology and Anatomy, and [3]Interdisciplinary Stem Cell Institute, University of Miami Miller School of Medicine, Miami, Florida, USA. [4]Department of Internal Medicine, [5]Department of Pediatrics, and [6]Charles and Jane Pak Center for Mineral Metabolism and Clinical Research, University of Texas Southwestern Medical Center, Dallas, Texas, USA. [7]Division of Nephrology, Department of Medicine, School of Medicine and Department of Epidemiology, School of Public Health, University of Alabama at Birmingham, Birmingham, Alabama, USA. [8]Department of Molecular and Cellular Pharmacology and Department of Medicine, University of Miami Miller School of Medicine, Miami, Florida, USA. [9]Renal Unit, Department of Medicine, Massachusetts General Hospital, Harvard Medical School, Boston, Massachusetts, USA. [10]Department of Pathology, University of Miami Miller School of Medicine, Miami, Florida, USA. [11]Department of Medicine, Jesse Brown VA Medical Center and University of Illinois Medical Center, Chicago, Illinois, USA. [12]Center for Management of Complex Chronic Care, Edward Hines Jr., VA Hospital, Hines, Illinois, USA. [13]Epidemiological Cardiology Research Center, Department of Epidemiology and Prevention, Wake Forest University School of Medicine, Winston Salem, North Carolina, USA. [14]Department of Medicine, Tulane School of Medicine, New Orleans, Louisiana, USA. [15]Division of Research, Kaiser Permanente Northern California and Departments of Epidemiology, Biostatistics and Medicine, UCSF, San Francisco, California, USA. [16]Renal, Electrolyte and Hypertension Division, Department of Medicine, [17]Center for Clinical Epidemiology and Biostatistics, and [18]Cardiology Division, Department of Medicine, University of Pennsylvania School of Medicine, Philadelphia, Pennsylvania, USA. [19]Department of Internal Medicine, University of Michigan Health Systems, Ann Arbor, Michigan, USA. [20]Section of Nephrology and Kidney Transplantation, Department of Internal Medicine, Temple University School of Medicine, Philadelphia, Pennsylvania, USA. [21]Department of Internal Medicine D and [22]Department of Cardiology and Angiology, University of Münster, Münster, Germany. [23]Department of Molecular Biology, [24]Department of Physiology, and [25]Department of Pathology, University of Texas Southwestern Medical Center, Dallas, Texas, USA. [26]National Institute of Diabetes and Digestive and Kidney Diseases, Bethesda, Maryland, USA.

Chronic kidney disease (CKD) is a public health epidemic that increases risk of death due to cardiovascular disease. Left ventricular hypertrophy (LVH) is an important mechanism of cardiovascular disease in individuals with CKD. Elevated levels of FGF23 have been linked to greater risks of LVH and mortality in patients with CKD, but whether these risks represent causal effects of FGF23 is unknown. Here, we report that elevated FGF23 levels are independently associated with LVH in a large, racially diverse CKD cohort. FGF23 caused pathological hypertrophy of isolated rat cardiomyocytes via FGF receptor–dependent activation of the calcineurin-NFAT signaling pathway, but this effect was independent of klotho, the coreceptor for FGF23 in the kidney and parathyroid glands. Intramyocardial or intravenous injection of FGF23 in wild-type mice resulted in LVH, and klotho-deficient mice demonstrated elevated FGF23 levels and LVH. In an established animal model of CKD, treatment with an FGF–receptor blocker attenuated LVH, although no change in blood pressure was observed. These results unveil a klotho-independent, causal role for FGF23 in the pathogenesis of LVH and suggest that chronically elevated FGF23 levels contribute directly to high rates of LVH and mortality in individuals with CKD.

Introduction

Chronic kidney disease (CKD) is a global public health problem that is estimated to affect approximately 26 million Americans and many more individuals worldwide (1). The presence of CKD increases risk of premature death, and cardiovascular disease is the leading cause at all stages of CKD (2). Left ventricular hypertrophy (LVH) is an important mechanism of cardiovascular disease in CKD that contributes to diastolic dysfunction, congestive heart failure, arrhythmia, and sudden death (3). Compared with a prevalence of 15%–21% in the general population (4), LVH affects 50%–70% of patients during intermediate stages of CKD and up to 90% of patients by the time they reach dialysis (5–7). Although traditional risk factors, such as chronic hypertension, contribute to high rates of LVH in CKD, the regression of LVH after kidney transplantation suggests other CKD-specific risk factors that remain poorly defined (8, 9). Discovery of additional mechanisms of LVH is needed to identify novel therapeutic targets for reducing the burden of cardiovascular disease in CKD.

The family of FGFs consists of 23 proteins that regulate cell proliferation, migration, differentiation, and survival (10). FGF2 is the prototypical FGF. It is expressed by many cell types, including cardiomyocytes and fibroblasts, which also express FGF receptors (FGFRs) (11, 12). FGF2 causes cardiac hypertrophy by inducing changes in gene expression that are simi-

Authorship note: Christian Faul, Ansel P. Amaral, and Behzad Oskouei contributed equally to this work.

Conflict of interest: Tamara Isakova has served as a consultant and received honoraria from Shire. Orlando M. Gutiérrez has received honoraria from Genzyme. Sylvia E. Rosas has received research support from Abbott Laboratories. Makoto Kuro-o has received research support from Ardelyx and Genzyme and honoraria from Amgen and Genzyme. Myles Wolf has served as a consultant or received honoraria from Abbott Laboratories, Amgen, Ardelyx, Baxter, Cytochroma, Genzyme, Luitpold Pharmaceuticals Inc., Novartis, Mitsubishi, and Shire.

Citation for this article: *J Clin Invest.* 2011;121(11):4393–4408. doi:10.1172/JCI46122.

lar to those caused by chronic pressure overload (13–16). This results in "pathological" LVH that is characterized by increased extracellular matrix deposition, hypertrophy, and apoptosis of individual myocytes and increased risk of congestive heart failure and death (17). The calcineurin–nuclear factor of activated T cells (calcineurin-NFAT) and MAPK signaling cascades are central regulators of pathological hypertrophy (18–20), which is distinct from "physiological" hypertrophy that occurs as an appropriate adaptive response to aerobic conditioning or pregnancy (17). In these settings, activation of phosphoinositide-3-kinase–Akt (PI3K-Akt) signaling stimulates growth of cardiomyocytes in the absence of excessive extracellular matrix deposition or myocyte apoptosis (17, 21).

FGF23 is the most recently discovered FGF (22). Unlike FGF2 and other canonical FGFs, which exert their paracrine and autocrine effects by binding heparan sulfate in the extracellular matrix (23), topological differences in the heparin-binding region of FGF23 enable it to avoid capture in the extracellular matrix (24). As a result, FGF23 functions as an endocrine hormone that regulates phosphorus homeostasis through binding to FGFR and klotho, its coreceptor in the kidney and parathyroid glands (25, 26). The primary physiological actions of FGF23 are to augment phosphaturia by downregulating expression of sodium-phosphate cotransporters in the renal proximal tubule and to decrease circulating concentrations of 1,25-dihydroxyvitamin D by inhibiting renal expression of the 1,25-dihydroxyvitamin D–synthesizing CYP27B1 (1-α-hydroxylase) and stimulating expression of the catabolic CYP24 (24-hydroxylase) (27, 28).

Circulating concentrations of FGF23 increase progressively as the renal capacity for phosphorus excretion declines (29). FGF23 levels are often 2- to 5-fold above the normal range during early and intermediate stages of CKD, but can reach levels 1,000-fold above normal in advanced renal failure (30, 31). While compensatory increases in FGF23 levels help patients with CKD to maintain normal serum phosphate levels, despite even severely reduced renal function (30), recent prospective studies of CKD and non-CKD patients demonstrated a dose-dependent association between elevated FGF23 levels and greater risks of major cardiovascular events and mortality (32–35). A plausible explanation linking high FGF23 to greater cardiovascular risk was offered by studies in which elevated FGF23 was independently associated with greater left ventricular mass and greater prevalence of LVH (36, 37). However, these small cross-sectional studies were unable to determine whether FGF23 directly contributes to LVH or is simply a biomarker of toxicity of other factors. In this report, we investigate the role of FGF23 in the pathogenesis of LVH in human and experimental studies. Using a large, nationally representative, racially diverse cohort of patients with CKD, we confirm that FGF23 levels and rates of LVH are elevated in CKD and that elevated FGF23 is independently associated with LVH. We demonstrate that FGF23 directly induces pathological hypertrophy of isolated cardiomyocytes and that mice develop LVH after intraventricular or intravenous injection of FGF23. We report that klotho-deficient mice, an established animal model for constitutively elevated FGF23 levels, develop LVH, and klotho heterozygotes manifest FGF23 levels and an LVH phenotype that are intermediate between those of wild-type and klotho-deficient mice. Finally, we demonstrate that administering an FGFR blocker to the 5/6 nephrectomy rat model of CKD attenuates the severity of LVH, without reducing the animals' markedly elevated blood pressure. These results establish a direct causal role for elevated FGF23 in the pathogenesis of LVH and suggest a novel mechanism to explain the high rates of LVH in patients with CKD.

Results

Circulating FGF23 levels are increased in CKD and independently associated with LVH. We measured FGF23 levels in baseline plasma samples from 3,070 individuals who underwent echocardiography 1 year later as part of the prospective Chronic Renal Insufficiency Cohort (CRIC) study. The participant population was 46% women, 42% black, and 13% Hispanic, with a median age of 60 years, median blood pressure of 125/71 mmHg, and a median estimated glomerular filtration rate of 42 ml/min/1.73 m^2. The median plasma FGF23 level of 142 RU/ml was more than 3-fold greater than that in previous studies of predominantly non-CKD populations (Figure 1A and ref. 34). The mean (± SEM) left ventricular ejection fraction was 54% ± 0.2%, left ventricular mass indexed to height$^{2.7}$ (LVMI) was 52 ± 0.3 g $m^{-2.7}$ (normal range, <50 in men; <47 in women), and LVH was present in 52% of participants.

The left ventricular ejection fraction was modestly lower in the highest versus the lower quartiles of FGF23 levels (Figure 1B), while the LVMI increased with increasing FGF23 quartiles (Figure 1C). Each unit increase in natural log-transformed FGF23 (lnFGF23) was associated with a 5.0 g $m^{-2.7}$ greater LVMI (95% CI, 4.4–5.7; $P < 0.001$). The prevalence of normal left ventricular geometry decreased with increasing quartiles of FGF23, while the prevalence of eccentric and concentric LVH increased (Figure 1D). Each unit increase in lnFGF23 was associated with a 2.5-fold greater relative risk (RR) of eccentric hypertrophy and concentric hypertrophy (95% CI, 2.1–3.0; $P < 0.001$) compared with normal ventricular geometry.

Multivariable analyses that adjusted for age, sex, race, ethnicity, weight, smoking, systolic blood pressure, history of cardiovascular disease, diabetes, total cholesterol, estimated glomerular filtration rate, hemoglobin, albuminuria, parathyroid hormone (PTH), and serum phosphate demonstrated that elevated FGF23 was independently associated with increased LVMI (1.5 g $m^{-2.7}$ greater LVMI per unit increase in lnFGF23, 95% CI, 0.8–2.2; $P < 0.001$) and conferred greater risk of eccentric and concentric LVH (RR 1.5 per unit increase in lnFGF23; 95% CI, 1.3–1.9; $P < 0.001$). In addition to elevated FGF23, older age, black race, Hispanic ethnicity, prior history of cardiovascular disease, higher blood pressure and body weight, and higher levels of proteinuria were also associated with eccentric and concentric LVH in the full multivariable model. The independent association between higher FGF23 and LVH was not modified by gender, race, ethnicity, CKD stage, treatment with antihypertensive agents, or a history of hypertension, diabetes, or prior cardiovascular events (data not shown). Furthermore, the results were unchanged when we adjusted for levels of 25-hydroxyvitamin D and 1,25-dihydroxyvitamin D in the subset of 1,342 participants for whom these were available (data not shown). These results indicate a robust association between FGF23 and LVH in patients with CKD across a broad range of kidney function.

Elevated FGF23 is associated with increased risk of new-onset LVH in CKD. Next, we prospectively examined whether elevated FGF23 is a risk factor for new-onset LVH in the 411 CRIC participants, who had normal left ventricular geometry on their baseline echocardiogram and underwent a second study 2.9 ± 0.5 years later. Eighty-four participants (20%) developed new-onset LVH. Elevated FGF23 levels at baseline were associated with increased future risk of new-onset LVH when FGF23 was expressed on a continuous scale (RR 2.4 per

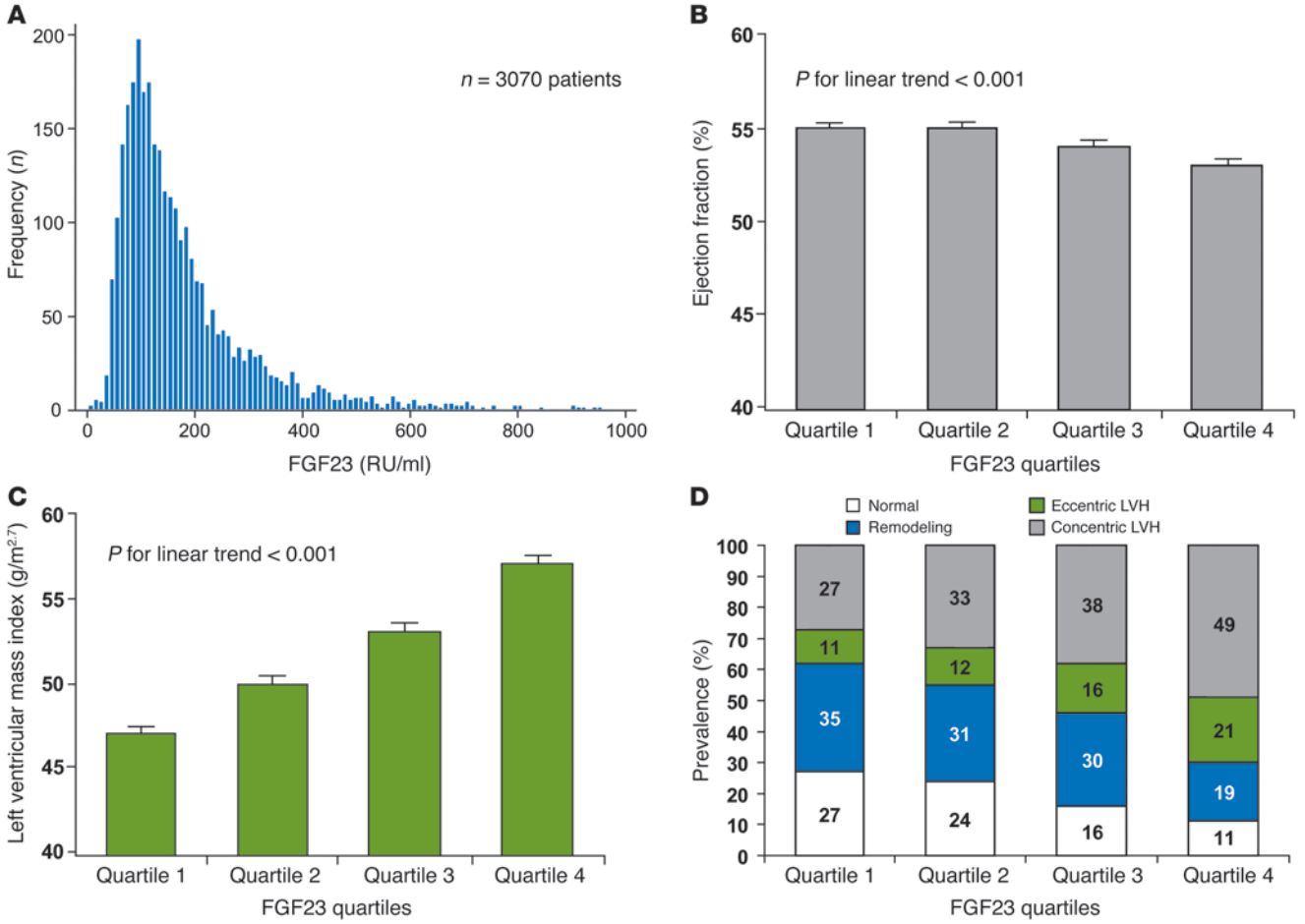

Figure 1

Elevated circulating FGF23 levels are associated with LVH in patients with CKD. (**A**) The distribution of FGF23 levels in baseline samples of 3,070 participants who enrolled in the CRIC study and underwent echocardiography 1 year later. The median FGF23 was 142 RU/ml. Fifty-eight participants with FGF23 of more than 1,000 RU/ml (range 1,054–14,319 RU/ml), who were included in the analysis, are not shown here. (**B**) Ascending quartiles of FGF23 were associated with significantly decreased ejection fraction (*P* for linear trend < 0.001), but the differences between groups were modest, and the mean (± SEM) ejection fraction for each quartile was normal (>50%). (**C**) Ascending quartiles of FGF23 were associated with significantly increased mean (± SEM) left ventricular mass index (*P* for linear trend < 0.001). (**D**) With increasing quartiles of FGF23, the prevalence of concentric (gray) and eccentric (green) LVH increased at the expense of normal left ventricular geometry (white) and left ventricular remodeling (blue) (*P* < 0.001). Numbers in the bars represent the percentages of prevalence for each condition.

unit increase in lnFGF23; 95% CI, 1.6–3.6; *P* < 0.001) or in categories (RR 2.4 for the highest versus the lower FGF23 quartiles; 95% CI, 1.3–4.3; *P* = 0.004). Among the 411 CRIC participants with follow-up echocardiograms, 138 had no history of hypertension, 18 (13%) of whom developed new-onset LVH. Within the normotensive subgroup, each unit increase in lnFGF23 was associated with a 4.4-fold greater risk of new-onset LVH (95% CI, 1.8–10.6; *P* = 0.001), and the highest FGF23 quartile had a 7.0-fold greater risk compared with that of the lower quartiles (95% CI, 2.1–23.6; *P* = 0.002). These data confirm that elevated FGF23 levels can precede the development of LVH in patients with CKD with and without hypertension.

FGF23 induces hypertrophy and activates prohypertrophic gene programs in isolated neonatal cardiomyocytes. We tested the hypothesis that the independent association between elevated FGF23 levels and increased risk of LVH in patients with CKD is mediated by a direct effect of FGF23 on cardiomyocytes. We compared the response of isolated neonatal rat ventricular cardiomyocytes (NRVMs) to 48 hours of treatment with FGF23 versus FGF2 at concentrations that induced hypertrophy in previous studies of FGF2 (13, 38). Since the development of LVH involves an increase in the contractile machinery and thus sarcomere number (17), we analyzed the expression of α-actinin, which anchors actin filaments to the sarcomeric Z-disc (39). Immunocytochemical and morphometric analyses revealed a dose-dependent, significant increase in cell surface area in response to FGF23 and FGF2 (Figure 2, A and B), while immunoblotting showed an increase in α-actinin protein levels (Figure 2C), indicative of increased sarcomeric content. In contrast to FGF23 and FGF2, we observed no change in the size of cardiomyocytes in response to FGF4 (data not shown).

Since these findings suggest induction of hypertrophic growth of NRVMs, we used RT-PCR analysis to determine expression levels of established markers of pathological cardiac hypertrophy after FGF treatment (Figure 2D). Expression of adult α–myosin heavy chain (α-*MHC*) decreased while expression of fetal β–myosin heavy chain (β-*MHC*) increased after FGF23 and FGF2 treatment. This switch

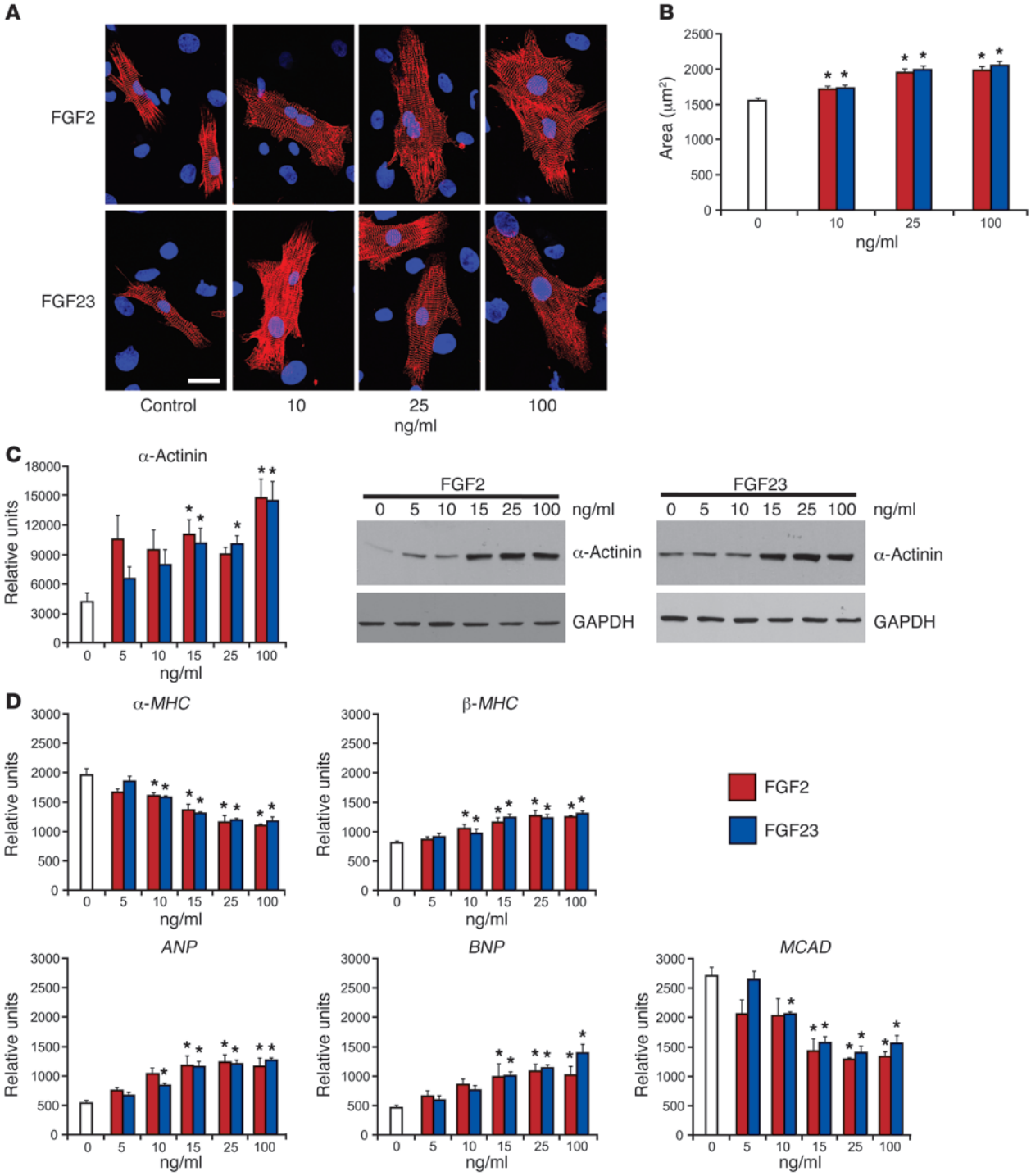

Figure 2

FGF23 increases the surface area of isolated NRVMs and activates hypertrophic gene programs. (**A**) Surface area of isolated NRVMs increases after FGF23 and FGF2 treatment, as revealed by immunocytochemical analysis using antibodies to α-actinin (red). DAPI (blue) identifies nuclei (original magnification, ×100; scale bar: 25 μm). (**B**) Compared with that of untreated control cells (white), 48 hours of treatment with FGF23 (blue) or FGF2 (red) significantly increases cell surface area (mean ± SEM). Fifty cells per group per isolation were analyzed by morphometry ($n = 3$ isolations of NRVMs; $^*P < 0.01$, compared with untreated). (**C**) Compared with those of untreated control cells (white), FGF23 (blue) or FGF2 (red) significantly increase α-actinin protein levels normalized to GAPDH in isolated NRVMs, as determined by immunoblotting (mean ± SEM; $n = 3$ isolations of NRVMs; $^*P < 0.01$). (**D**) Compared with that of untreated control cells (white), FGF23 (blue) or FGF2 (red) decrease expression of α-*MHC* and *MCAD* mRNA and increase β-*MHC*, *ANP*, and *BNP*) mRNA (mean ± SEM; $n = 3$ isolations of NRVMs quantified by RT-PCR normalized to *Gapdh*; $^*P < 0.01$, compared with untreated).

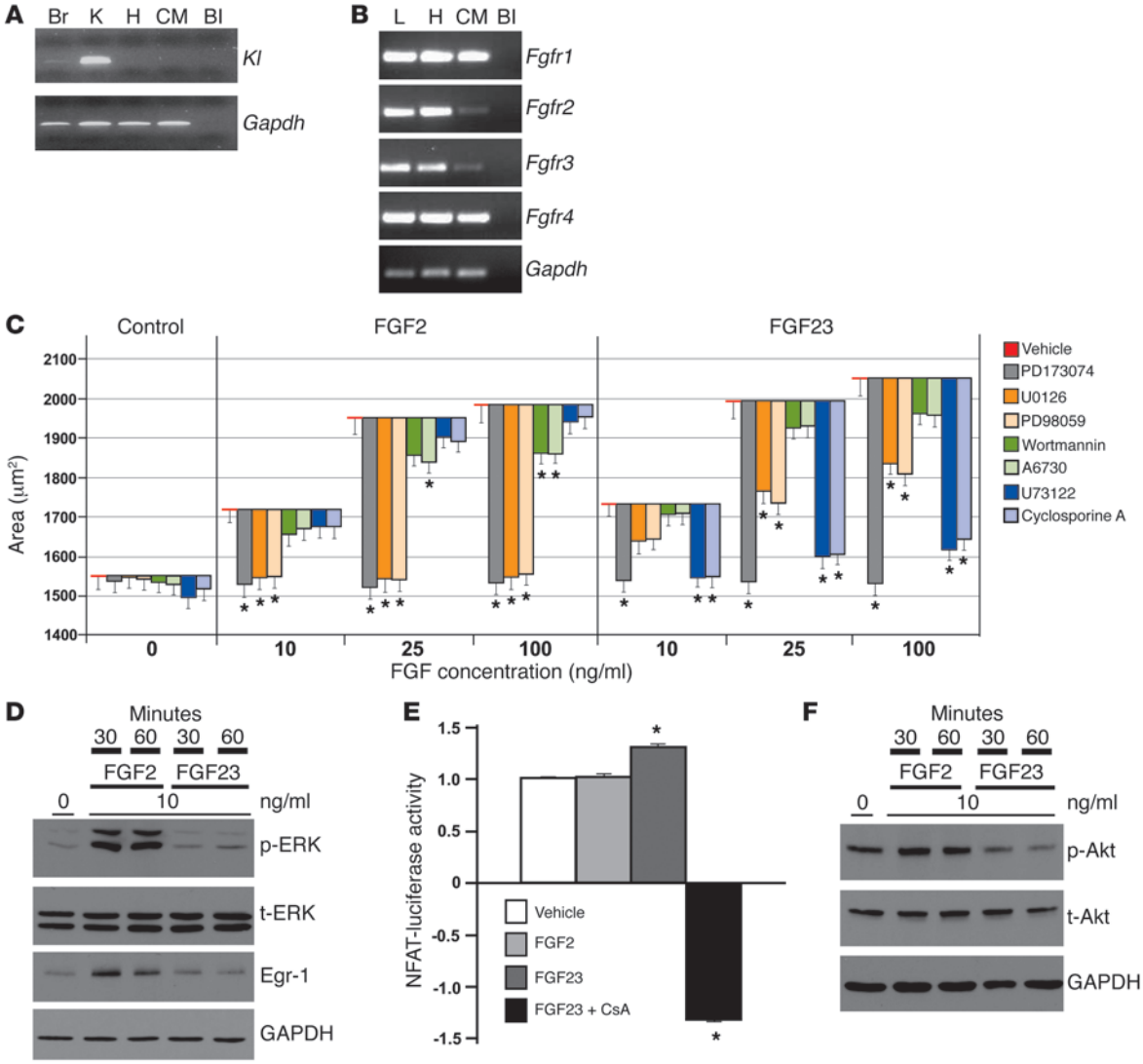

Figure 3

FGF23 and FGF2 use different signaling pathways to induce hypertrophy of NRVMs. (**A**) Klotho expression is detectable in mouse brain (Br) and kidney (K) by nested RT-PCR but not in heart (H), isolated cardiomyocytes (CM), or in the absence of template (blank [Bl]). (**B**) FGFR1–FGFR4 are detectable in liver (L), heart, and isolated cardiomyocytes by RT-PCR but not in the absence of template. (**C**) Surface area of isolated NRVMs after 48 hours of FGF treatment alone and in the presence of inhibitors. The lower edge of the bars represents the mean (± SEM) area, and their height represents the difference in area compared with that of cells that were treated with FGF alone (red). Inhibiting FGFR (gray) prevents any increase in area regardless of FGF concentration. ERK inhibition (orange shades) completely prevents FGF2-induced hypertrophy but only partially prevents FGF23-induced hypertrophy. PI3K/Akt inhibition (green shades) partially prevents FGF2-induced hypertrophy but has no effect on FGF23-treated cells. PLCγ/calcineurin inhibition (blue shades) prevents FGF23-induced hypertrophy but not FGF2-induced hypertrophy (150 cells per condition; $*P < 0.01$, compared with corresponding FGF concentration without inhibitor). (**D**) FGF2 stimulates a greater increase in ERK phosphorylation (p-ERK) and Egr-1 expression than FGF23 relative to total ERK (t-ERK). (**E**) FGF23 but not FGF2 increases NFAT activity in C2C12 myoblasts. Cyclosporine A (CsA) blocks the effect of FGF23 (values represent fold change ± SEM compared with vehicle; $*P < 0.01$, compared with vehicle). (**F**) Only FGF2 induces an increase in Akt phosphorylation (p-Akt) relative to total Akt (t-Akt).

from adult to fetal MHC isoforms indicates reactivation of fetal gene programs that are associated with cardiac hypertrophy (40–43). In addition, FGF23 and FGF2 treatment increased expression of atrial natriuretic peptide (*ANP*) and brain natriuretic peptide (*BNP*), which are established markers of LVH (43, 44). FGF23 and FGF2 treatment also decreased expression of medium chain acyl-CoA dehydrogenase (*MCAD*), an enzyme that regulates fatty acid oxidation. Cardiomyocytes that undergo hypertrophy shift their primary energy source from fatty acids to carbohydrates (45), which is marked by reduced expression of MCAD (46). Collectively, these data demonstrate that FGF23 exerts direct hypertrophic effects on isolated NRVMs.

FGF23-mediated hypertrophy is FGFR dependent but klotho independent. Klotho is the primary coreceptor for FGF23 in the kidney and parathyroid glands, but it is not expressed in cardiomyocytes (25, 47). To confirm that the observed hypertrophic response of NRVMs to FGF23 treatment was independent of klotho, we analyzed klotho

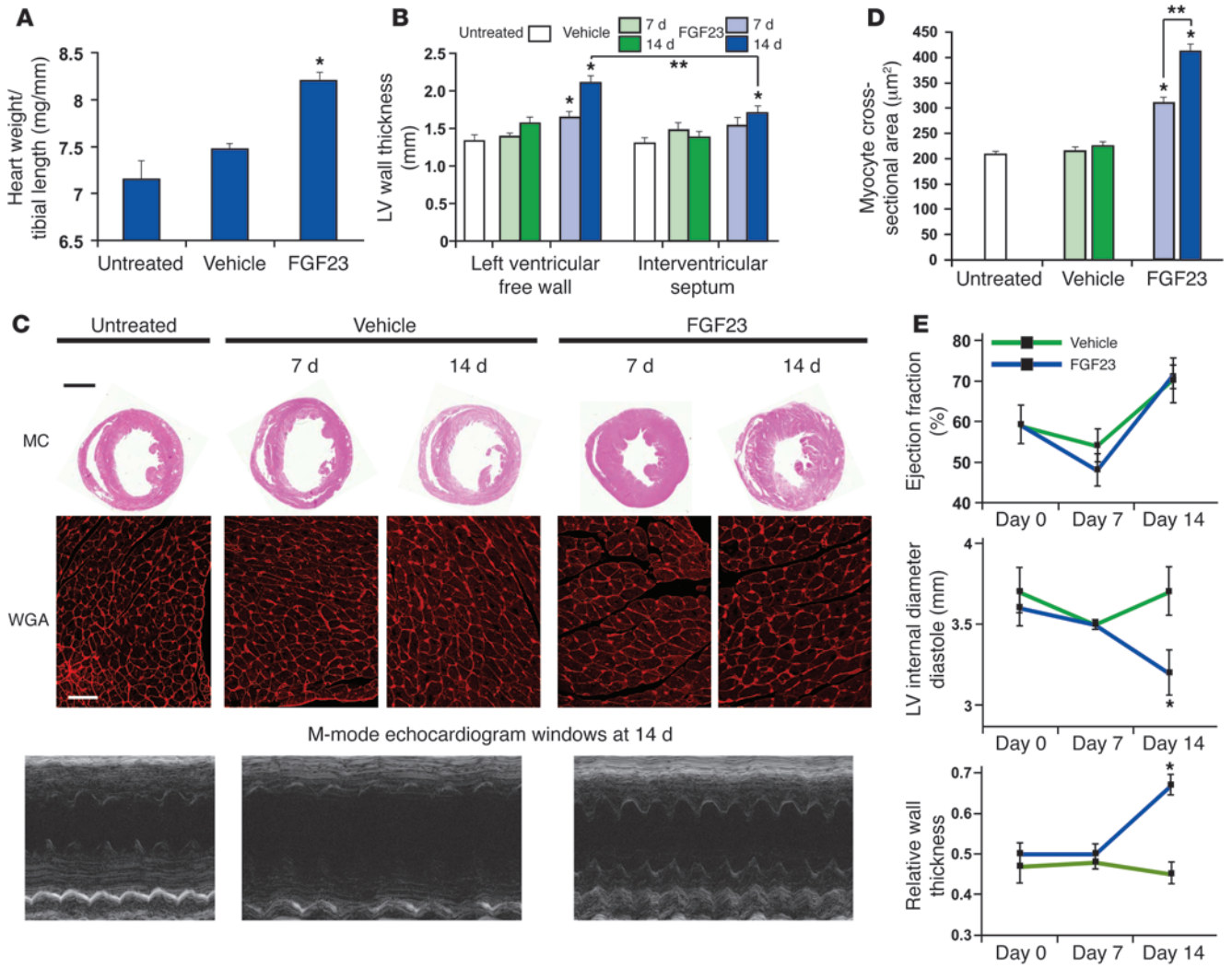

Figure 4

Intramyocardial injection of FGF23 induces LVH in mice. (**A**) Intramyocardial injection of FGF23 induces a significantly increased ratio of heart weight to tibial length by day 14 (*$P < 0.01$, compared with vehicle). (**B**) Intramyocardial injection of FGF23 induces significantly increased thickness of the left ventricular free wall that is detectable at day 7 and progresses by day 14. Hypertrophy is significantly more pronounced at the injection site in the free wall compared with the interventricular septum at 14 days (*$P < 0.01$, compared with vehicle at corresponding date and site; **$P < 0.01$, comparing free wall to septum). (**C**) Representative gross pathology section from the cardiac mid-chamber (MC; hematoxylin and eosin stain; original magnification, ×5; scale bar: 200 μm) and WGA-stained sections from the mid-chamber free wall (original magnification, ×63; scale bar: 50 μm) demonstrate FGF23-indcued LVH at 14 days, confirmed by M-mode echocardiography. (**D**) Intramyocardial injection of FGF23 induces significantly increased cross-sectional surface area of individual cardiomyocytes (*$P < 0.01$, compared with vehicle; **$P < 0.01$, comparing day 14 versus 7). (**E**) Echocardiography at baseline and at 1 and 2 weeks after injection of FGF23 or vehicle reveals no change in ejection fraction but significantly decreased left ventricular internal diameter in diastole and increased relative wall thickness by day 14 in the mice injected with FGF23, consistent with concentric LVH (*$P < 0.01$, compared with vehicle). All values are mean ± SEM; $n = 3$ mice per group for morphological analyses; $n = 100$ cells per group for WGA analysis.

expression by nested RT-PCR using 2 sets of klotho-specific primers in 2 consecutive PCRs in order to detect even the smallest amounts of cDNA. We detected klotho (*Kl*) mRNA in mouse brain and kidney, which are known to express the protein (25), but not in isolated NRVMs or total heart preparations (Figure 3A).

The biological functions of FGFs are mediated by FGFR1–FGFR4, which are members of the receptor tyrosine kinase family (48). FGF23 can bind the FGFR isoforms with varying affinity (49, 50), and we detected expression of all isoforms in liver, isolated NRVMs, and total murine heart (Figure 3B). To determine, whether the prohypertrophic effect of FGF23 on cardiomyocytes is dependent on FGFR, we cotreated isolated NRVMs with FGF23 or FGF2 and the pan-FGFR inhibitor PD173074 (51). The presence of PD173074 blocked FGF23- and FGF2-induced increases in cell surface area, regardless of FGF concentration (Figure 3C). These findings demonstrate that FGF23 induces hypertrophy of isolated NRVMs via FGFR activation but through a klotho-independent pathway.

Activation of isolated NRVMs by FGF23 and FGF2 uses distinct signaling pathways. FGFR signaling involves activation of the MAPK cascade, in which the ERK plays a central role (10, 52). Once phosphorylated

in cardiomyocytes, ERK activates a wide array of targets (19, 53, 54), including the early growth response 1 (Egr-1) transcription factor (55), and additional downstream target genes that promote hypertrophy. Since FGF2 uses ERK as a downstream mediator of its hypertrophic effect in cardiomyocytes (56), and FGF23 signals via ERK activation in its primary target cells (25, 26), we tested whether FGF23 also activates ERK in isolated NRVMs. As expected, FGF2 stimulated a robust increase in phosphorylated ERK, the activated kinase form, while total ERK levels did not change (Figure 3D). In addition, FGF2 stimulated an increase in Egr-1 expression levels (Figure 3D). In contrast, we detected only a modest increase in phosphorylated ERK and Egr-1 levels in isolated NRVMs treated with FGF23 (Figure 3D). Consistent with these data, when we cotreated isolated NRVMs with the ERK inhibitors U0126 or PD98059, FGF2-induced hypertrophy was completely prevented, whereas FGF23-induced hypertrophy was only partially diminished (Figure 3C). These data suggest that, whereas the MAPK cascade is a dominant signaling pathway of FGF2-mediated cardiac hypertrophy, FGF23 appears to use additional signaling pathways.

To identify alternative signaling cascades underlying FGF23-induced hypertrophy of cardiomyocytes, we studied PLCγ, which is another downstream mediator of FGFR signaling (10). Treatment with the PLCγ inhibitor, U73122, attenuated FGF23-mediated hypertrophy but had no effect on FGF2-treated cells (Figure 3C). The calcineurin-NFAT cascade is an important downstream target of PLCγ (57) that is involved in pathological LVH (43, 58). The presence of the calcineurin inhibitor, cyclosporine A, attenuated FGF23-mediated hypertrophy to a virtually identical extent as U73122 but had no effect on FGF2-treated cells (Figure 3C). Consistent with the inhibitor data, FGF23 but not FGF2 treatment significantly increased NFAT activity in C2C12 myoblasts stably transfected with an NFAT-responsive luciferase reporter (59), while the presence of cyclosporine A blocked the effect (Figure 3E). These data indicate that the PLCγ-calcineurin-NFAT axis is a dominant signaling pathway of FGF23-mediated hypertrophy of NRVMs.

Finally, we analyzed the PI3K-Akt signaling axis, which has been implicated in the development of physiological rather than pathological hypertrophy of cardiomyocytes (17, 60). The presence of the PI3K inhibitor, wortmannin, or the Akt inhibitor, A6730, partially attenuated FGF2-induced hypertrophy but did not significantly alter hypertrophic growth of FGF23-treated cells (Figure 3C). Consistent with this finding, FGF2 but not FGF23 stimulated a modest increase in phosphorylated Akt, the activated kinase form (Figure 3F). Based on these data, we conclude that activation of the PI3K-Akt signaling cascade is not involved in FGF23-mediated cardiac hypertrophy.

Direct myocardial delivery of FGF23 induces LVH in mice. To determine whether the direct prohypertrophic effect of FGF23 on isolated NRVMs could be replicated in vivo, we injected recombinant FGF23 protein directly into the left ventricular myocardium of mice. Using a standard procedure for implanting stem cells into murine hearts in vivo (61), we delivered 7.5 ng FGF23 dissolved in 30 μl PBS, or 30 μl PBS alone, via 3 separate injection sites (10 μl each) into the anterior wall of the left ventricle of adult wild-type mice. This approach allowed the direct delivery of FGF23 into the myocardium and thereby minimized confounding by FGF23-induced changes in circulating concentrations of other mineral metabolites that are regulated by FGF23 and could impact the development of LVH. Serologic testing confirmed minimal systemic absorption of FGF23, as there was no increase in serum levels of FGF23, and there were no significant differences in serum phosphate, calcium, PTH, or creatinine between the FGF23- and vehicle-injected animals at days 7 and 14 after injection (data not shown).

The ratio of heart weight to tibial length, an established measure of cardiac hypertrophy (62–64), was significantly increased at day 14 after FGF23 injection compared with that after vehicle injection (Figure 4A). Compared with vehicle, FGF23 induced a significant increase in left ventricular free wall thickness at day 7, which increased further by day 14 (Figure 4B). Thickness of the interventricular septum was also significantly increased by day 14 after FGF23 injection compared with that after vehicle injection, but the thickness of the ventricular free wall, in which FGF23 was injected, was significantly greater than the septum at day 14 (Figure 4B). This suggests a gradient of effect related to the proximity to the injection sites in which the concentration of FGF23 was likely highest. Representative gross pathology tissue sections demonstrated FGF23-mediated LVH characterized by thickened ventricular walls and reduced internal chamber diameter (Figure 4C). Microscopic analysis of cardiomyocytes stained with a fluorochrome-labeled wheat germ agglutinin (WGA) revealed a significant increase in cross-sectional surface area, indicating hypertrophic growth of individual myocytes (Figure 4, C and D). Echocardiography data revealed no change in ejection fraction over time in FGF23- or vehicle-injected mice, but left ventricular internal diameter in diastole was significantly decreased, while relative wall thickness (ratio of wall thickness to internal chamber diameter) was increased by day 14 in the mice injected with FGF23 (Figure 4, C and E). Consistent with the in vitro results, cardiac injections of FGF23 caused a decrease in α-*MHC* and *MCAD* mRNA levels and an increase in expression of β-*MHC*, *ANP*, and *BNP* (data not shown). In addition, *Kl* was not detected in the mouse hearts at baseline, and its expression was not induced at 7 or 14 days after injection (data not shown). From these data, we conclude that FGF23 directly induces LVH in vivo independently of klotho.

High systemic levels of FGF23 result in LVH in mice. The local concentration of FGF23 in the left ventricle after intramyocardial injection was likely substantially higher than in physiological and pathological states. Therefore, we administered FGF23 protein intravenously to determine whether systemically elevated FGF23 levels could also induce LVH. We injected 40 μg/kg of recombinant FGF23 protein dissolved in 200 μl of PBS into the tail vein of adult wild-type mice twice daily for 5 days, with 8 hours between daily doses. This dose of FGF23 was chosen based on published reports in which a similar dose stimulated ERK phosphorylation and increased Egr-1 expression in klotho-expressing target organs of FGF23 (25). The frequency of injections was chosen based on a pharmacokinetic study of adult wild-type rats, in which we injected a single dose of 40 μg/kg FGF23. The half-life of circulating FGF23 was 30 minutes, and serum levels remained elevated above baseline at 4 hours after injection (data not shown). Therefore, we estimated that 2 daily injections of 40 μg/kg would likely produce elevated FGF23 levels for at least 8 hours per day in mice. Control animals underwent the same injection schedule using 200 μl of PBS alone. On the morning of day 6, serum was collected for assay of FGF23, mice were sacrificed, and the hearts were examined.

Serum FGF23 levels measured at the time of sacrifice (16 hours after the final injection) were significantly increased compared with those of vehicle-injected mice (Figure 5A), which indicates that FGF23 levels

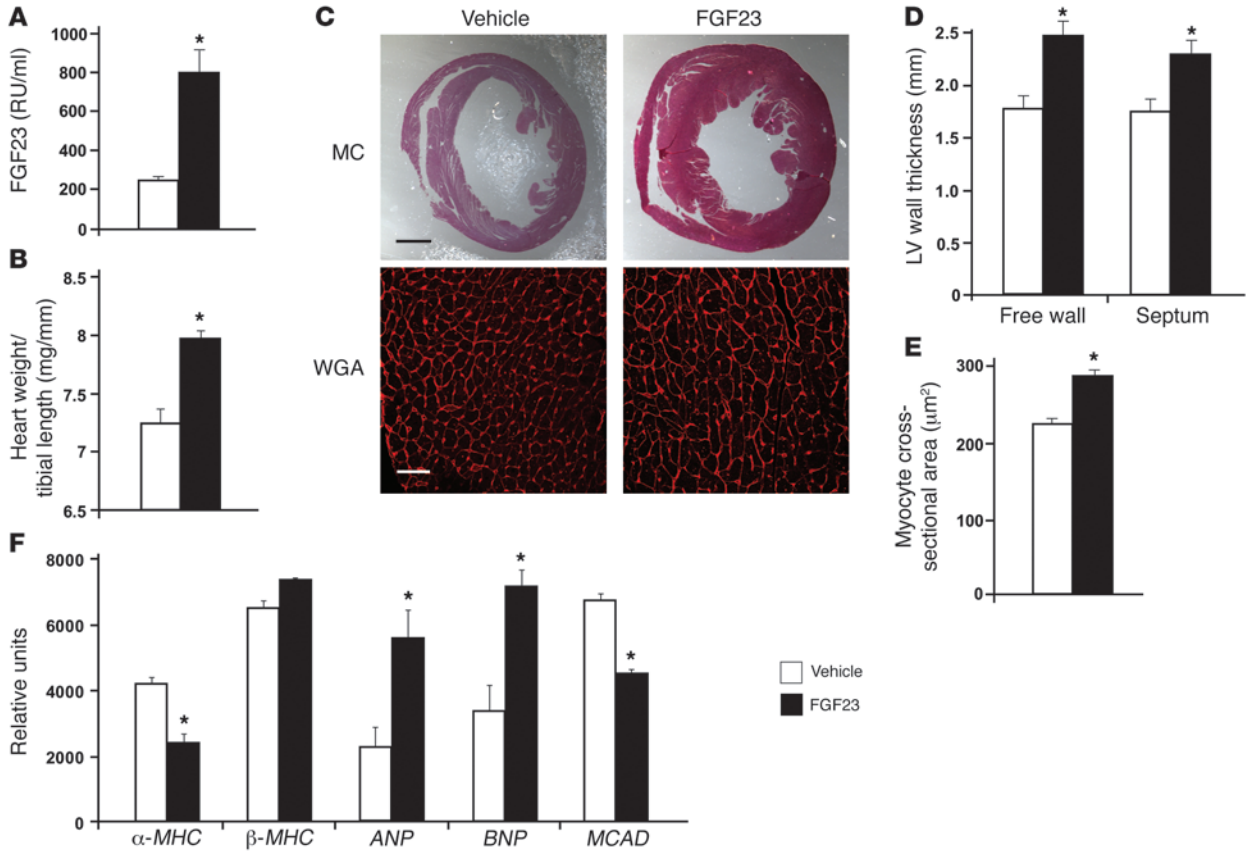

Figure 5

Intravenous injection of FGF23 results in LVH in mice. (**A**) Intravenous injection of FGF23 results in a significant increase in serum FGF23 levels (mean ± SEM; n = 11 mice per group; *P < 0.01, compared with vehicle). (**B**) Intravenous injection of FGF23 results in a significant increase in cardiac weight/tibial length (mean ± SEM; n= 11 mice per group; *P < 0.01, compared with vehicle). (**C**) Representative gross pathology (hematoxylin and eosin stain; original magnification, ×5; scale bar: 200 μm) and WGA-stained sections (original magnification, ×63; scale bar: 50 μm) from the mid-chamber of the left ventricle demonstrate LVH in mice that received intravenous injections of FGF23. (**D**) Mice that received intravenous injections of FGF23 manifest a significant increase in left ventricular wall thickness (mean ± SEM; n = 5 mice per group; *P < 0.01, compared with vehicle). (**E**) Mice that received intravenous injections of FGF23 manifest a significant increase in cross-sectional surface area of individual cardiomyocytes (mean ± SEM; n = 100 cells per group; *P < 0.01, compared with vehicle). (**F**) Intravenous injection of FGF23 results in a significant decrease in expression of α-*MHC* and *MCAD* mRNA and increased β-*MHC*, *ANP*, and *BNP* mRNA (mean ± SEM; n = 3 mice per group quantified by RT-PCR normalized to *Gapdh*; *P < 0.05, compared with vehicle).

were likely persistently elevated throughout the study period. Compared with vehicle-injected mice, FGF23-injected mice developed a significantly increased ratio of heart weight to tibial length (Figure 5B), increased left ventricular wall thickness (Figure 5, C and D), increased cross-sectional surface area of individual cardiomyocytes (Figure 5, C and E), increased expression of *ANP* and *BNP* mRNA levels, and decreased expression of α-*MHC* and *MCAD* (Figure 5F). These results demonstrate that intravenous injection of FGF23 increases serum levels and yields an LVH phenotype that is similar to that induced by direct intramyocardial injection of FGF23.

LVH develops in a genetic mouse model of elevated FGF23. To determine whether LVH develops in a murine model of constitutively elevated FGF23 levels, we analyzed klotho-deficient (*kl/kl*) and klotho heterozygous (*kl/+*) mice. Kidneys of *kl/kl* mice are resistant to the phosphaturic effect of FGF23, which results in significant increases in circulating FGF23 levels (25). Consistent with previous studies (47), *kl/kl* mice were significantly smaller (9.7 ± 0.2 g) than *kl/+* mice (25.3 ± 0.7 g) and wild-type mice (24.3 ± 0.5 g; P < 0.01 for each comparison) at 12 weeks of age. Serum FGF23 levels were more than 15-fold elevated in *kl/kl* mice and 3-fold elevated in *kl/+* mice compared with those in wild-type mice (Figure 6A). Serum 1,25-dihydroxyvitamin D and phosphate levels were also significantly elevated in *kl/kl* mice compared with those in wild-type mice but not in *kl/+* mice (Figure 6A). There were no significant differences in PTH levels among genotypes (data not shown). Blood pressure did not differ at 6 weeks of age between *kl/+* mice and wild-type mice (109 ± 11 mmHg versus 107 ± 9 mmHg) but was significantly higher in *kl/+* mice than in wild-type mice at 12 weeks (123 ± 14 mmHg versus 108 ± 11 mmHg; P < 0.05). Due to their small size, we could not measure blood pressure in *kl/kl* mice.

Representative pathology sections at 12 weeks of age demonstrated LVH in *kl/kl* mice compared with wild-type mice (Figure 6B). Although absolute left ventricular wall thickness was highest for *kl/+* mice, followed by *kl/kl* mice, and then wild-type mice (Figure 6C), the ratio of cardiac weight standardized to total body weight was highest in *kl/kl* mice (Figure 6D). When compared with that of

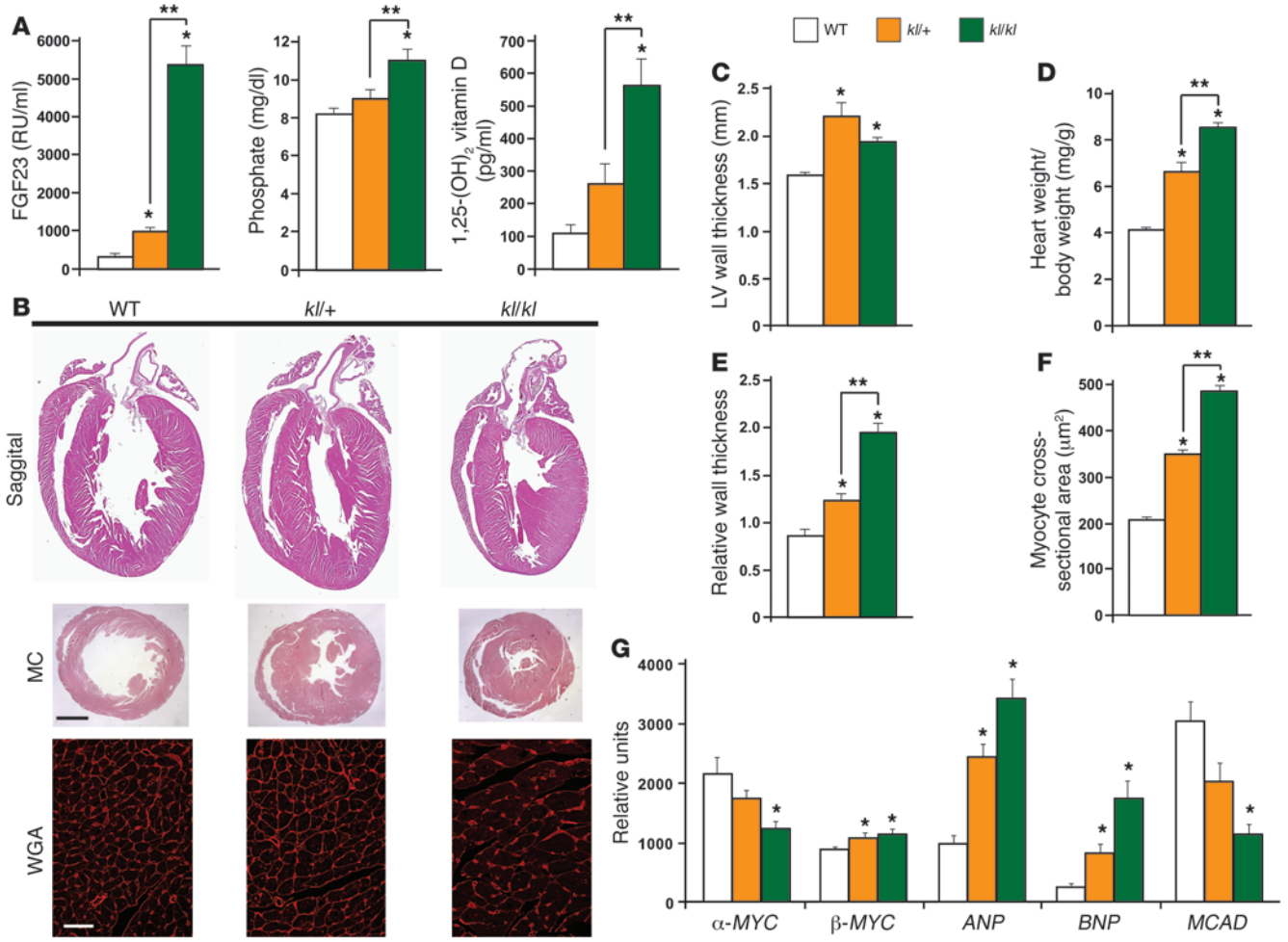

Figure 6

Klotho-deficient and klotho heterozygous mice develop LVH. (**A**) *kl/kl* mice demonstrate significant increases in serum levels of FGF23, phosphate, and 1,25-dihydroxyvitamin D compared with those of wild-type mice. Only FGF23 was significantly increased in *kl/+* mice. (**B**) Representative gross pathology of sagittal and mid-chamber sections of the heart (hematoxylin and eosin stain; original magnification, ×5; scale bar: 200 μm) and WGA-stained sections from the left ventricular mid-chamber free wall (original magnification, ×63; scale bar: 50 μm) demonstrate LVH in *kl/kl* and *kl/+* mice. (**C**) *kl/kl* and *kl/+* mice manifest significant increases in left ventricular wall thickness. (**D**) *kl/kl* and *kl/+* mice manifest significant increases in the ratio of heart weight to total body weight. (**E**) *kl/kl* and *kl/+* mice manifest significant increases in left ventricular relative wall thickness. (**F**) *kl/kl* and *kl/+* mice manifest significant increases in cross-sectional surface area of individual cardiomyocytes. (**G**) *kl/kl* and *kl/+* mice demonstrate decreased levels of α-*MHC* and *MCAD* mRNA and increased β-*MHC*, *ANP*, and *BNP* mRNA. All values are mean ± SEM ($n = 6$ mice per group for all laboratory and morphological analyses; $n = 3$ mice per group for RT-PCR analyses; $n = 100$ cells per group for WGA analysis; *$P < 0.01$, compared with WT; **$P < 0.01$, compared with *kl/+*).

wild-type mice, *kl/kl* mice manifested significantly increased relative wall thickness (Figure 6E), increased cross-sectional surface area of individual cardiomyocytes (Figure 6F), and changes in gene expression that are characteristic of LVH and similar to those we observed in NRVMs and mice that underwent intramyocardial or intravenous injection of FGF23 (Figure 6G). Interestingly, morphological WGA staining and mRNA analyses of *kl/+* mice also revealed an LVH phenotype but in a pattern that was intermediate between *kl/kl* and wild-type mice (Figure 6, B–G). These results demonstrate that an established genetic animal model of elevated serum FGF23 levels develops LVH in a dose-dependent fashion.

FGFR activity is required for the development of LVH in a rat model of CKD. Since the cardiac effects of FGF23 are mediated by FGFR activation and could be blocked in vitro by the FGFR inhibitor PD173074, we tested the hypothesis that PD173074 could also attenuate LVH in the 5/6 nephrectomy rat model of CKD, which is known to develop increased FGF23 levels, severe hypertension, and LVH (65, 66). We performed 5/6 nephrectomy in male Sprague Dawley rats using standard surgical techniques (65) and administered by intraperitoneal injection either 1 mg/kg body weight/d of PD173074 dissolved in PBS ($n = 6$) or vehicle alone ($n = 6$), beginning 1 hour after surgery and continued daily for 14 days. As a negative control, 6 rats underwent sham nephrectomy. At day 14 after surgery, we measured blood pressure, performed echocardiograms, collected blood for laboratory testing, sacrificed the animals, and examined their hearts.

Immunoblotting revealed decreased hepatic expression of p-ERK protein levels in the rats that received PD173074 compared with those in the sham and 5/6 nephrectomized rats, indicating effective

Table 1
Compared with sham, 5/6 nephrectomy results in impaired renal function, hypertension, and elevated serum FGF23 levels that are unchanged by FGFR inhibition

	Sham	5/6 nephrectomy	
		Vehicle	PD173074
	(*n* = 6)	(*n* = 6)	(*n* = 6)
Serum creatinine (mg/dl)	0.24 ± 0.01	0.46 ± 0.04[A]	0.49 ± 0.07[A]
Blood urea nitrogen (mg/dl)	16.5 ± 0.7	39.8 ± 8.2[A]	30.3 ± 4.3[A]
Creatinine clearance (ml/min/100 g)	0.91 ± 0.1	0.35 ± 0.1[A]	0.39 ± 0.1[A]
Systolic blood pressure (mmHg)	135 ± 4	197 ± 9[A]	208 ± 13[A]
FGF23 (RU/ml)	119 (37–163)	1,497 (377–10,452)[A]	1,136 (370–5,097)[A]

Values are reported as mean ± SEM or median (25th–75th percentiles). [A]$P < 0.05$, compared with sham.

blockade of canonical FGFR-dependent MAPK signaling (data not shown). Renal function was significantly impaired and serum FGF23 levels were significantly elevated in the animals that underwent 5/6 versus sham nephrectomy, but there were no differences between the 5/6 nephrectomized animals that received PD173074 or vehicle (Table 1). Similarly, blood pressure was markedly increased in animals that underwent 5/6 versus sham nephrectomy, but no difference was detected between the 5/6 nephrectomy groups (Table 1).

The 5/6 nephrectomized animals that received vehicle developed LVH compared with those that received sham surgery, but LVH was significantly attenuated in the animals that were injected with PD173074. Compared with vehicle treatment, PD173074 treatment led to decreased left ventricular mass, reduced ratio of heart weight to total body weight, decreased left ventricular wall thickness and relative wall thickness, decreased cross-sectional surface area of individual cardiomyocytes, and increased left ventricular end diastolic volume and ejection fraction (Figure 7, A–C). Compared with sham, 5/6 nephrectomy led to increased cardiac expression of β-*MHC* and *ANP* and decreased expression of *MCAD* mRNA levels, each of which was not observed in PD173074-injected animals (data not shown). These data indicate that blocking FGFR attenuates the development of LVH in a well-established animal model of CKD with elevated FGF23 levels, despite having no effect on the severity of CKD or hypertension.

Discussion

In the largest human study of FGF23 and cardiac structure to date, we confirm previous reports of an independent association between elevated FGF23 levels and greater risk of LVH, which was present in 52% of patients compared with 15%–21% of the general population (4). In a prospective analysis of those patients with CKD who had normal left ventricular geometry at baseline, elevated FGF23 levels were also associated with increased future risk of new-onset LVH. Using in vitro studies and complementary animal models, we extended these results by demonstrating that FGF23 causes pathological cardiac hypertrophy directly. We showed that the cardiac hypertrophic effects of FGF23 are mediated by FGFR-dependent activation of the calcineurin-NFAT signaling cascade but do not require klotho as coreceptor. We further demonstrated that blocking FGFR signaling can prevent LVH independently of blood pressure in an established animal model of CKD that is characterized by elevated FGF23 levels, severe hypertension, and LVH. By demonstrating direct pathological effects of FGF23 on the heart, we believe that these data uncover a novel mechanism of LVH and novel aspects of the biology of FGF23 that reposition it from biomarker of cardiovascular risk to mechanism of disease and, thus, potential target for clinical intervention.

Klotho is a transmembrane protein expressed primarily in the kidney and parathyroid glands, in which it acts as a coreceptor to increase the binding affinity of FGF23 for FGFR (25, 26). In addition, a circulating soluble form of klotho that is derived from cleavage of the extracellular domain or alternative splicing acts as an endocrine hormone involved in calcium and phosphate homeostasis (67). Although it has been assumed that FGF23 cannot exert biologically relevant effects in the absence of klotho, we demonstrate that FGF23 induces hypertrophy of cardiomyocytes that do not express klotho and is associated with LVH in mice that lack klotho. The observation of LVH in klotho-deficient mice is particularly important, because it minimizes the likelihood that soluble klotho acted as a coreceptor for FGFR signaling in the mice that developed LVH after intramyocardial and intravenous injection of FGF23. Another finding which be believe to be novel is that klotho heterozygotes manifest FGF23 levels and a cardiac phenotype that are intermediate between those of klotho-deficient mice and wild-type mice. Unlike klotho-deficient mice, LVH develops in the heterozygotes in the absence of a significant increase in serum phosphate. The identification of dose-response effects for both FGF23 levels and endowment of normal klotho gene copies that are independent of serum phosphate strengthens our results.

In its classic target organs, FGF23 binds FGFR-klotho complexes and activates the MAPK cascade, leading to increased ERK activation and Egr-1 expression (25, 27, 47). The widely held view that other organs are not capable of responding to FGF23 emerged from studies that defined FGF23 responsiveness based on presence or absence of organ-specific activation of ERK and Egr-1 after intravenous administration of FGF23 (25, 68). We confirm that FGF23 does not increase cardiac expression of Egr-1 (25); however, it exerts biological effects nonetheless. We conclude that analyses of klotho expression, ERK activity, or Egr-1 expression alone may be inadequate reporter assays to assess FGF23 responsiveness. Furthermore, since the presence of klotho is not an absolute prerequisite for biological activity of FGF23, we believe our results open new avenues for investigating FGF23 "toxicity" in other nonclassic target organs.

We propose 2 mechanisms to explain klotho-independent, FGF23-induced LVH. First, low-affinity binding of FGF23 to FGFR (50, 69) may be adequate to induce LVH when there is a protracted period of cardiac exposure to high concentrations of FGF23, such as in CKD. FGF23 toxicity may be accentuated further in patients with CKD in whom klotho expression is downregulated in the kidney and parathyroid glands (67, 70), which could enhance promiscuous binding of FGF23 to FGFR in other tissues. Thus, high circulating FGF23 concentrations combined with decreased klotho expression could represent an especially cardiotoxic blend in patients with CKD. Alternatively, FGF23-induced LVH could be mediated by higher-affinity binding to specific cardiac FGFRs, such as FGFR4, which we and others detected in isolated cardiomyocytes and in total heart tissue (71). Unlike FGFR1–FGFR3, FGFR4 is

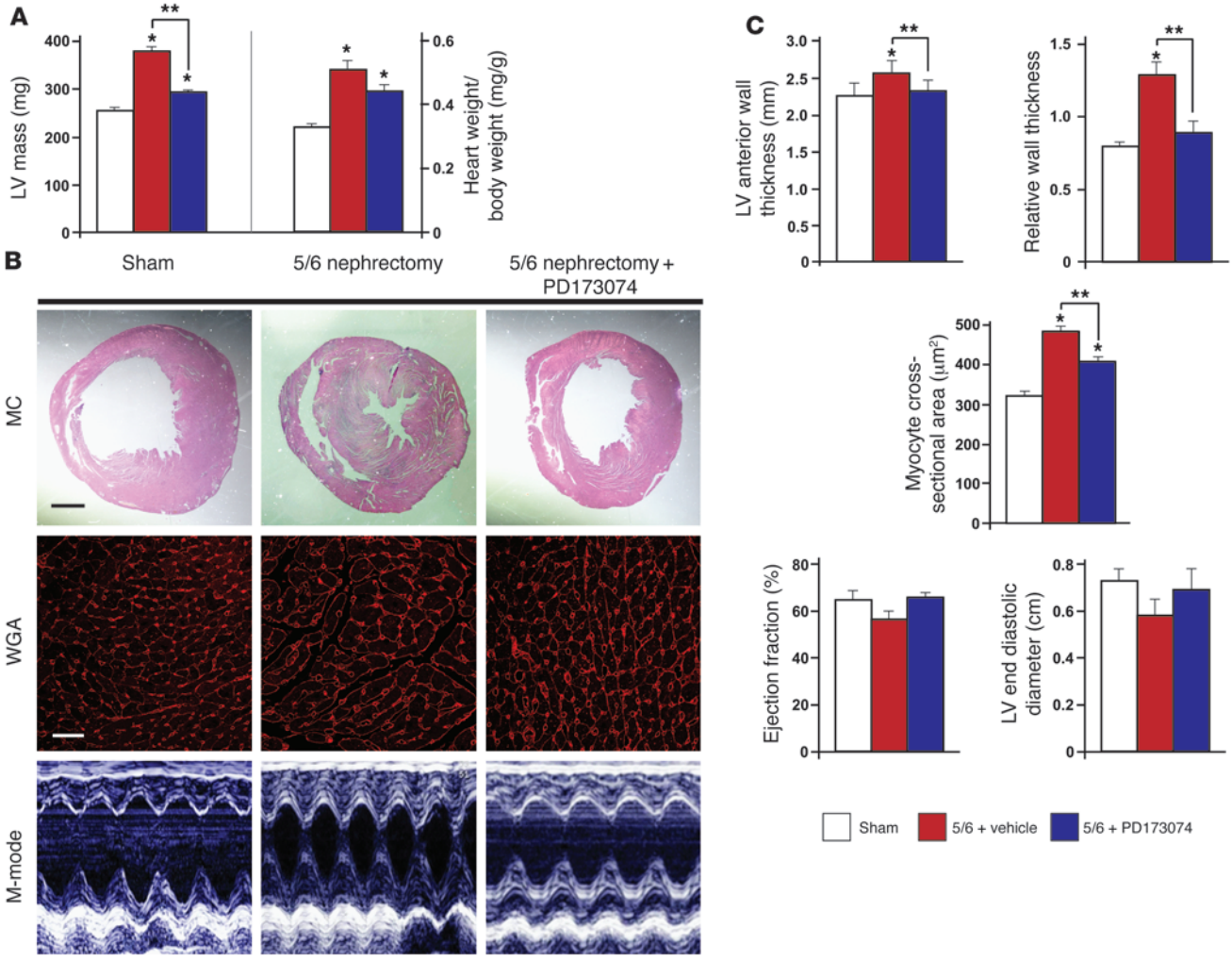

Figure 7

Pharmacological inhibition of FGFR attenuates LVH in an animal model of CKD. (**A**) PD173074 attenuates the increases in left ventricular mass (by echocardiography) and cardiac weight/body weight that develop in 5/6 nephrectomized rats treated with vehicle (*$P < 0.05$, compared with sham; **$P < 0.05$, compared with 5/6 nephrectomy treated with vehicle). (**B**) Representative gross pathology sections (hematoxylin and eosin stain; original magnification, ×2.5; scale bar: 400 μm), M-mode echocardiography images, and WGA-stained sections (original magnification, ×63; scale bar: 50 μm) from the left ventricular mid-chamber at day 14 after 5/6 nephrectomy demonstrate that PD173074 attenuates LVH compared with vehicle. (**C**) PD173074 attenuates the effects of 5/6 nephrectomy to increase left ventricular anterior wall thickness and relative wall thickness (by gross pathology), to increase cross-sectional surface area of individual cardiomyocytes (by WGA staining), and to decrease ejection fraction and LV end diastolic volume (by echocardiogram; *$P < 0.05$, compared with sham; **$P < 0.05$, compared with 5/6 nephrectomy treated with vehicle). All values are mean ± SEM ($n = 6$ rats per group).

capable of binding FGF23 with high affinity even in the absence of klotho, similar to the other endocrine FGFs in its subfamily, FGF19 and FGF21 (49, 72). Additional studies are needed to determine which specific FGFR mediates the cardiac effects of FGF23.

Although FGF23 and FGF2 induce a similar hypertrophic phenotype in isolated NRVMs, they use different downstream signaling pathways. FGF2-induced hypertrophy depends primarily on activation of ERK, whereas FGF23-induced hypertrophy is partially ERK dependent but primarily requires PLCγ-calcineurin-NFAT activation. The PI3K-Akt pathway appears to contribute only modestly to FGF2- and not to FGF23-induced hypertrophy. Based on these findings, we conclude that FGF23 and FGF2 cause pathological hypertrophy by activating different branches of canonical FGFR signaling in the heart (Figure 8). To our knowledge, this is the first study to identify an FGF that induces cardiac PLCγ-calcineurin-NFAT signaling, which is a classic signaling cascade in pathological LVH (58). A recent report, in which cyclosporine attenuated LVH in uremic rats (65) that are known to have elevated FGF23 levels (66), lends further indirect support to the central role of this pathway.

In contrast to CKD, in which FGF23 levels rise as a secondary response to impaired phosphate excretion, X-linked hypophosphatemia (XLH) is a prototypical disease of primary FGF23 excess (73). Data on cardiac structure in XLH are sparse and inconsistent, with one but not all studies reporting a high rate of LVH (74). We can speculate several possibilities to reconcile these findings with ours. Patients with CKD are often older and harbor several cardiovascular risk factors. This could accentuate the prohypertrophic effects of FGF23 relative to XLH, which primarily affects children

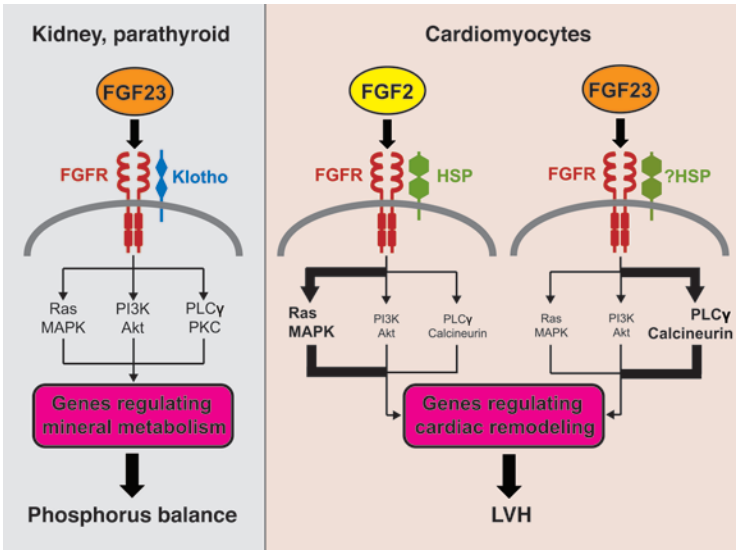

Figure 8
Schematic representation of FGF23 signaling in classic target cells and cardiomyocytes. In the kidney and parathyroid glands, FGF23 signaling requires FGFR and the coreceptor klotho. FGF23-klotho binding to FGFR stimulates autophosphorylation of the receptor tyrosine kinase and induces signaling through 3 major pathways: Ras-MAPK, PI3K-Akt, and PLCγ-PKC. FGF23 regulates phosphorus balance by altering expression of genes involved in parathyroid, vitamin D, and phosphorus metabolism. In cardiomyocytes, FGF2 signaling requires FGFR and heparan sulfate proteoglycans (HSP) as coreceptor and signals primarily through the Ras-MAPK pathway. Binding of FGF23 to FGFR on cardiomyocytes stimulates autophosphorylation of the receptor tyrosine kinase independent of klotho, which is not expressed in cardiomyocytes, and signals primarily through the PLCγ-calcineurin pathway. Whether HSP acts as coreceptor remains to be determined.

with few cardiovascular risk factors. Second, the magnitude of the increase in FGF23 levels is typically less dramatic in XLH than in CKD (30, 73). Perhaps variably increased FGF23 levels in XLH might explain their variable manifestation of LVH. Finally, hypophosphatemia and severe phosphate depletion are associated with impaired cardiac function (75, 76). Therefore, phosphate depletion in XLH could modulate the cardiac response to FGF23 relative to that in CKD, in which phosphate levels are normal to high. Additional studies are needed to explore these possibilities.

While many factors are involved in the complex pathogenesis of LVH, the results of this study indicate that FGF23 is one contributing molecular mediator. Given the strong association between LVH and future mortality (77) and the growing number of patients with CKD with elevated FGF23 levels and high rates of LVH, these data suggest that a component of cardiovascular risk in patients with CKD could be directly attributable to FGF23. However, quantifying the magnitude of effect of elevated FGF23 levels on LVH relative to that of other risk factors, such as hypertension, will require placebo-controlled randomized trials of FGF23 reduction. Our finding that blocking FGFR attenuates LVH in a classic animal model of CKD without altering the animals' severe hypertension suggests an important blood pressure–independent, cardiac effect of FGF23. These mechanistic data lend support for a randomized trial to test whether dietary phosphorus restriction or administration of phosphate binders that reduce FGF23 (78), or monoclonal antibodies or small molecules that block its actions (79), can slow the progression of LVH, reduce cardiovascular events, and improve survival in patients with CKD.

Methods

Human study

Study population. The CRIC study is a multicenter prospective cohort study of individuals with non-dialysis-dependent CKD that is designed to identify risk factors for cardiovascular disease and progression of CKD (80). A total of 3,939 participants aged 21 to 74 years, with estimated glomerular filtration rate of 20–70 ml/min/1.73 m^2, were enrolled. Black and Hispanic participants were oversampled so that the CRIC population resembled the demographics of CKD in the United States. Participants were excluded if they were unable to provide consent, institutionalized, pregnant, or enrolled in other studies; suffered from polycystic kidney disease, New York Heart Association class III–IV heart failure, HIV, cirrhosis, or active malignancy; or underwent recent chemotherapy, immunosuppressive therapy, prior organ transplantation, or treatment with dialysis for more than 1 month. Complete data on baseline FGF23 levels and LVMI measured by echocardiograms that were performed 1 year later were available in 3,070 participants. There was no difference in the distribution of FGF23 levels between patients with and without data on left ventricular mass. Follow-up echocardiograms were available at a subsequent study visit in 411 participants who had normal left ventricular geometry on their baseline echocardiogram.

Assays. FGF23 was measured in duplicate after a single thaw of stored baseline plasma specimens using a second generation C-terminal enzyme-linked immunosorbent assay (Immutopics). The total inter- and intra-assay coefficient of variation was 7.6% at 308 RU/ml. Although this assay theoretically detects both intact FGF23 and its C-terminal fragments, since virtually all circulating FGF23 is intact, the C-terminal assay measures biologically active FGF23 (31). We used liquid chromatography–mass spectroscopy to measure 25-hydroxyvitamin D levels and competitive chemiluminescent immunoassays to measure 1,25-dihydroxyvitamin D levels in 1,342 participants, using serum samples that were collected at the study visit when the first echocardiograms were performed.

Echocardiography. Two-dimensional transthoracic echocardiograms were obtained using standard American Society of Echocardiography protocols (81). Studies were performed locally at each study site, recorded digitally, and analyzed at the Echo Core Lab at the University of Pennsylvania using dedicated software (Tomtec Inc.). Ventricular dimensions, wall thickness, and relative wall thickness were measured at end-diastole and end-systole using 2D techniques. Ejection fraction was calculated from measured diastolic and systolic volumes. Left ventricular mass was indexed to height$^{2.7}$, as recommended by American Society of Echocardiography standards, and calculated from 2D images using the 5/6 area-length method (81). LVH was defined as LVMI ≥ 50 g $m^{-2.7}$ in men or ≥ 47 g $m^{-2.7}$ in women (81). Relative wall thickness was defined as 2 × posterior wall $\text{thickness}_{\text{diastole}}$/left ventricular internal $\text{diameter}_{\text{diastole}}$, with normal values < 0.45 (81). Left ventricular geometry was categorized as normal (normal LVMI, normal relative wall thickness), concentric remodeling (normal LVMI, high relative wall thickness), eccentric LVH (high LVMI, normal relative wall thickness), or concentric LVH (high LVMI, high relative wall thickness) (81).

Statistics. We used linear regression to examine the association between lnFGF23 and LVMI and generalized logistic regression to simultaneously analyze the odds of eccentric and concentric hypertrophy relative to normal ventricular geometry. We modeled FGF23 on a continuous scale after natural log transformation was used to achieve normality and in quartiles that were defined by its distribution in the overall study population. We tested for linear trends across quartiles of FGF23 and used multivariable analyses to adjust for demographic, clinical, and laboratory characteristics and to test for effect modification by gender, race, ethnicity, CKD stage, diabetes status, and prior cardiovascular disease. Analyses were performed using Intercooled Stata 11, and *P* values of less than 0.05 were considered statistically significant.

Experimental studies

Growth factors. We used recombinant mouse FGF23 (6His-tagged Tyr25-Val251 [Arg179Gln]; 26.1 kDa), FGF2 (Ala11-Ser154; 16.2 kDa), and FGF4 (Ala30-Leu202) proteins (R&D Systems). We chose the mutant form of FGF23 because it is resistant to furin protease-mediated degradation, which prolongs the protein's half-life (82). We confirmed in vitro biological activity of FGF23 by detecting increased levels of phospho-ERK and Egr-1 in response to treatment with FGF23 in HEK293 cells that transiently express FLAG-tagged klotho (data not shown), as has been done previously (26). We confirmed in vivo biological activity of FGF23 by demonstrating decreased serum phosphate levels over 4 hours after a single intravenous injection of 40 μg/kg of purified protein dissolved in 0.5 ml of PBS in 3 male Sprague Dawley rats (Charles River; data not shown), as has been done previously (22).

Primers. See Supplemental Table 1 (supplemental material available online with this article; doi:10.1172/JCI46122DS1) for primer sequences.

Isolation and culture of NRVMs. NRVMs were isolated using a standard isolation system (Worthington Biochemical Corporation) (83). Hearts from 1- to 2-day-old Sprague Dawley rats were harvested and minced in calcium- and magnesium-free HBSS, and the tissue was digested with 50 μg/ml trypsin at 4°C for 20 to 24 hours. Soybean trypsin inhibitor in HBSS was added, and the tissue was further digested with collagenase (in Leibovitz L-15 medium) under slow rotation (0.1 *g*) at 37°C for 45 minutes. Cells were released by gently triturating the suspension 20 times with a standard 10-ml plastic serological pipette and filtering it twice through a cell strainer (70 μm, BD Falcon). Cells were incubated at room temperature for 20 minutes and spun at 100 *g* for 5 minutes. The cell pellet was resuspended in plating medium (DMEM [Cellgro] with 17% Media 199 [Invitrogen], 15% FBS [Invitrogen], and 1% penicillin/streptomycin solution [P/S; Invitrogen]). Cells were counted using a hemocytometer.

Cells were plated on glass and plastic surfaces, which were coated with laminin (Invitrogen; 10 μg/ml in PBS) at room temperature for 1 hour prior to plating. For immunofluorescence analysis, 1×10^6 cells were seeded per well on glass coverslips in 6-well plates. For protein and RNA isolation, 2×10^6 cells were seeded in 6-cm culture dishes. Cells were left undisturbed in plating medium at 37°C for 72 hours and then cultured in maintenance medium (DMEM with 20% Media 199, 1% insulin-transferrin-sodium selenite solution [ITS; Sigma-Aldrich], and 1% P/S) in the presence of 100 μM 5-bromo-2′-deoxyuridine (BrdU; Sigma-Aldrich) to eliminate proliferating nonmyocytes, resulting in a relatively pure population of isolated cardiomyocytes (84). After 4 days, isolated cardiomyocytes were cultured in BrdU-containing maintenance medium in the presence of recombinant murine FGF23, FGF2, or FGF4 for 48 hours.

RNA isolation and quantification. RNA was purified from isolated NRVMs using the RNeasy Kit (Qiagen) and from cardiac and renal tissue using 1 ml per 100 mg tissue TRIzol (Invitrogen) following the manufacturers' protocol. Prior to RT-PCR, total RNA samples were digested with DNase I (Roche), and RNA was transcribed into cDNA using SuperScript II (Invitrogen). For RT-PCR, 100 ng cDNA, AmpliTaq Gold DNA polymerase (Applied Biosystems), and sequence specific primers were used. Thirty cycles (95°C, 5 minutes; 53°C, 30 seconds; 72°C, 30 seconds) were run on a GeneAmp PCR System 9700 (Applied Biosystems), and reactions were analyzed on a 2% agarose gel. Ethidium bromide signals were captured with a Bio-Rad Gel Doc XR system and quantified by densitometry using ImageJ software (http://rsbweb.nih.gov/ij/). Values were normalized to GAPDH signals, and cDNAs from 3 independent experiments were analyzed. For nested PCR, 100 ng cDNA were used in the first run (15 cycles) with sequence-specific outside primers. Five percent of the reaction was used as template for the second run (25 cycles) with sequence-specific inside primers, and the total reaction was analyzed by agarose gel electrophoresis. Gene expression in rat tissue was analyzed by real-time PCR using the SYBR Green PCR Master Mix (Applied Biosystems), with the ABI PRISM 7700 Sequence Detection System. Relative expression values were evaluated with the $2^{-\Delta\Delta}$Ct method using *GAPDH* as housekeeping gene.

Protein isolation and immunoblotting. NRVMs were scraped from a 6-cm plate using 400 μl CHAPS extraction buffer (20 mM Tris-HCl, pH 7.5, 500 mM NaCl, 0.5% CHAPS, protease inhibitor cocktail [Roche], protein phosphatase inhibitors [Sigma-Aldrich]) and incubated on ice for 15 minutes. The cell lysate was centrifuged at 21,000 *g* and 4°C for 15 minutes, and the supernatant was boiled in sample buffer and analyzed by SDS-PAGE and immunoblotting, as described before (85, 86). For protein extraction from mouse hearts and rat liver, tissue was isolated, minced, and homogenized in CHAPS extraction buffer at 1:10 (w/v), and protein lysates were prepared as described above. Antibodies to sarcomeric α-actinin (EA-53; Sigma-Aldrich; 1:1,000), total (Cell Signaling Technology; 1:1,000) and phospho-ERK (Cell Signaling Technology; 1:1,000), total and phospho-Akt (Cell Signaling Technology; 1:1,000 and 1:2,000), and GAPDH (Abcam; 1:10,000) were used as primary antibodies, and horseradish peroxidase–conjugated goat anti-mouse and goat anti-rabbit (Promega; 1:20,000) were secondary antibodies.

Immunocytochemistry and morphometry. We analyzed isolated NRVMs on laminin-coated glass coverslips by immunocytochemistry according to our established protocols (85, 86). The mouse monoclonal antibody against sarcomeric α-actinin (EA-53; Sigma-Aldrich) was used at 1:1,000, and Cy3-conjugated goat anti-mouse (Jackson Immuno Research) was used as a secondary antibody at 1:750. To visualize nuclei, fixed cells were incubated with DAPI (400 ng/ml in PBS) for 5 minutes. Immunofluorescence images were taken on a Leica TCS-SP5 confocal microscope with a ×63 oil objective with a ×1.6 zoom. Leica AF6000 fluorescence software was used to measure the cell surface area based on α-actinin–positive staining.

To assess the signaling pathways involved in FGF23- and FGF2-mediated hypertrophy, we analyzed the morphometry of plated cells that were pretreated with specific inhibitors for 60 minutes prior to the addition of the FGFs at varying concentrations. The following inhibitors and concentrations were used: pan-FGFR, PD173074 (Sigma-Aldrich) at 10 nM; ERK1/2, U0126 (Cell Signaling Technology) at 10 μM; ERK1, PD98059 (Cell Signaling Technology) at 20 μM; PI3K, wortmannin (Cell Signaling Technology) at 500 nM; Akt1/2, A6730 (Sigma-Aldrich) at 200 nM; PLC and A_2, U73122 (Sigma-Aldrich) at 10 μM; calcineurin, cyclosporine A (Sigma-Aldrich) at 0.83 μM.

Myoblast NFAT reporter assays. C2C12 myoblasts that were stably transfected with the pHTS NFAT reporter vector (Biomyx) carrying a luciferase expression cassette under the control of 4 NFAT enhancer sites were a gift from Norbert Frey, University of Kiel, Kiel, Germany (59). NFAT-luciferase-C2C12 cells in 6-well plates were maintained in DMEM containing 10% FBS, 2 mM L-glutamine, penicillin/streptomycin, and 200 μg/ml of hygromycin B for selection and starved in 0.5% FBS containing medium 16 hours

prior to FGF treatment. Cells were incubated in FGF23 or FGF2 at 25 ng/ml for 60 minutes after pretreatment with or without cyclosporine A for 60 minutes. Chemiluminescence was detected and quantified in 1×10^5 cells using the Promega Bright-Glo assay according to the manufacturer's instructions and a Veritas Microplate Luminometer (Turner Biosystems). All experiments were conducted in triplicate.

Intramyocardial injections in mice. Twelve-week-old adult C57BL/6 mice (The Jackson Laboratory) underwent cardiac surgery using a standard operative procedure that has been described previously for intramyocardial implantation of stem cells (61). All procedures were performed by a single investigator who was blinded to the specific treatment group. Briefly, mice were anesthetized with isoflurane, and an incision was made between the third and fourth rib to reveal a cardiac window. Three injections of purified recombinant murine FGF23 in PBS or PBS alone were delivered into the free wall of the left ventricle via a 30-gauge needle attached to a standing Hamilton syringe. At each of the 3 sites, 10 μl were injected for a total of 30 μl containing a total of 7.5 ng FGF23. Cardiac function was evaluated by Vevo 770 echocardiography imaging system (Visual Sonics) at baseline and 2 weeks after surgery. Long- and short-axis 2D parasternal views and short-axis M mode views were recorded under general anesthesia, with isoflurane inhalation delivered through a nose mask. The heart rate was maintained above 400 bpm, with controlled body temperature set to 37°C. At 7- and 14-days after injection, animals were sacrificed, and hearts were isolated, perfused ex vivo (6 ml of 10% formalin with 4 ml of 20 mM KCl), stored overnight in 10% formalin for fixation, and then serially sectioned (7-μm slices) and stained with hematoxylin and eosin. Age-matched untreated animals were sacrificed at 14 weeks of life.

Intravenous injections in mice. Twelve-week-old adult C57BL/6 mice underwent tail vein injections using standard protocols as previously described for the systemic delivery of plasmid DNA (87). Briefly, mice were placed in a restrainer and 40 μg/kg FGF23 dissolved in 200 μl PBS were injected into the tail vein of 6 mice twice daily with 8 hours between injections for 5 consecutive days. Six mice underwent the same injection schedule using 200 μl PBS alone as negative control. On the morning of the sixth day, 16 hours after the final tail vein injections, animals were sacrificed, and the hearts were isolated and prepared using the same protocol as described above. The experiment was repeated with 6 additional animals per group. Since the results were similar in each experiment, combined results are presented.

Klotho mice. Klotho-deficient mice were generated with transgene integration into the *klotho* locus, leading to disruption of the 5′-flanking region and loss of expression as previously described (47). We analyzed homozygous (*kl/kl*), heterozygous (*kl/+*), and wild-type mice. We measured blood pressure using a computerized tail-cuff system (BP-2000, Visitech Systems) in conscious animals. Mice were trained for 3 consecutive days in the prewarmed (98°F ± 0.5°F) tail-cuff device to familiarize them with the procedure, followed by measurements of blood pressure everyday for 5 days. During each procedure, 10 trial cycles were repeated, and then 10 cycles were recorded per test. Four successful procedures were performed daily, and mean results for each animal from 5 consecutive days were reported. Animals were sacrificed at 8 weeks (for RNA isolation) or 12 weeks (for morphometry) of age, and the hearts were isolated and prepared using the same protocol as described above.

5/6 nephrectomy model of CKD. Kidney disease was induced in Sprague Dawley rats using the 5/6 nephrectomy method as described previously (65). Rats were randomized into 3 groups, with 6 animals per group: sham nephrectomy or 5/6 nephrectomy plus 14 daily intraperitoneal injections of vehicle (PBS) or PD173074 at 1 mg/kg/d, beginning 1 hour after surgery. High-resolution echocardiography (30 MHz) was performed at 14 days after surgery to assess wall and chamber dimensions, left ventricular mass, and left ventricular systolic function using an HDI 5000 Ultrasound system (Philips). M-mode, 2D, and 3D recordings were obtained under general anesthesia delivered through a nose mask while heart rate and body temperature were maintained. On day 14, animals were sacrificed, and the hearts were isolated and prepared for molecular, histological, and serological analyses, following the same protocols as described for mice. Expression levels of hypertrophic markers were determined by real-time PCR. We confirmed in vivo biological activity of PD173074 by detecting decreased levels of phospho-ERK in liver protein extracts by immunoblotting when compared with vehicle-treated animals.

Morphology and molecular analysis of mouse and rat hearts. Short-axis sections of hematoxylin and eosin–stained hearts were used to quantify myocardial thickness by measuring the distance from the inner to the outer myocardial edges at the mid-chamber zone. Mean left ventricular free wall thickness was calculated from 7 measurements of wall thickness taken at 0, 30, 60, 90, 120, 150, and 180 degrees along the hemicircle of the short axis of the free wall; the mean of 7 comparable measurements along the hemicircle of the short axis of the interventricular septum was used to calculate mean septal thickness. Since *kl/kl* mice display severe growth retardation with small hearts (47), we also measured relative wall thickness calculated as the ratio of 2 times the anterior wall thickness divided by left ventricular internal diameter; similar measurement were made on the 5/6 nephrectomized rats. Total RNA was isolated from flash frozen hearts using TRIzol (Invitrogen), and PCR analyses were performed as described above.

Fluorescence microscopy and morphometry. We measured cross-sectional surface area of cardiomyocytes in paraffin-embedded, short-axis sections of mouse and rat hearts. Briefly, 7-μm-thick sections were deparaffinized according to our established protocols (88). To specifically label cardiomyocytes, we used mouse monoclonal MF20 antibody against sarcomeric myosin (The Developmental Hybridoma Band, University of Iowa, Iowa City, Iowa, USA) (89) at 1:200 and Cy5-conjugated donkey anti-mouse (Invitrogen) as secondary antibody at 1:400. To visualize nuclei, fixed tissue was incubated with DAPI (400 ng/ml in PBS) for 5 minutes. To visualize cellular borders, fixed tissue was incubated with WGA conjugated to Alexa Fluor 555 (Invitrogen) at 1 mg/ml in PBS containing 10 mM sodium azide. Immunofluorescence images were taken on a Leica TCS-SP5 confocal microscope with a ×63 oil objective. Leica AF6000 fluorescence software was used to quantify cross-sectional cell surface area of 25 cells per field in 4 fields along the mid-chamber free wall based on WGA-positive staining.

Serology. Blood was collected from mice and rats at sacrifice via cardiac puncture and was centrifuged at 4°C and 21,000 *g* for 15 minutes. Serum supernatants were collected, stored at –80°C, and subsequently analyzed in batches for FGF23 (C-terminal mouse assay, Immutopics); PTH (1-84 assay, Alpco Immunoassays); and 1,25-dihydroxyvitamin D, phosphate, calcium, blood urea nitrogen, and creatinine (Ortho Vitros 250 Chemistry Analyzer).

Statistical analysis of in vitro and animal data. Data are presented as mean ± SEM. Analysis of variance and *t* tests were used for statistical inference, with 2-tailed *P* values of less than 0.05 considered significant.

Study approval

The human study protocol was approved by the institutional review boards at each of the primary sites of the CRIC study (see Supplemental Methods), and all participants provided written informed consent. All protocols and experimental procedures were approved by the Institutional Animal Care and Use Committees at the University of Miami Miller School of Medicine (intramyocardial and tail vein injections in mice), the University of Texas Southwestern Medical Center (klotho mice), and the University of Münster, Münster, Germany (5/6 nephrectomy in rats).

Acknowledgments

This study was supported by grants from the NephCure Foundation (to C. Faul), the American Heart Association (to C. Faul and M.C. Hu), the Charles and Jane Pak Center for Mineral Metabolism and Clinical Research, University of Texas Southwestern Medical Center (to M.C. Hu), the George M. O'Brien Kidney Research Core Center/UT Southwestern Medical Center at Dallas (NIH P30DK-07938 to O.W. Moe), the Stifterverband für die Deutsche Wissenschaft and Simon-Claussen-Stiftung (H 1405409999915626 to M. Brand), the Inter-disciplinary Research Initiative of the University of Miami Miller School of Medicine (to C. Faul, J.M. Hare, and M. Wolf), a Health Services Research and Development Service Career Development Award from the Department of Veterans Affairs (to M.J. Fischer), and grants F30DK091057 (to A.P. Amaral), K23DK087858 (to T. Isakova), K23DK081673 (to O.M. Gutierrez), R01DK091392 (to M.C. Hu, M. Kuro-o, and O.W. Moe), R01AG019712 (to M. Kuro-o), R01DK076116 (to M. Wolf), and R01DK081374 (to M. Wolf) from the National Institutes of Health. Funding for the CRIC study was obtained under a cooperative agreement from National Institute of Diabetes and Digestive and Kidney Diseases (grant no. 5U01DK060990, 5U01DK060984, 5U01DK06102, 5U01DK061021, 5U01DK061028, 5U01DK60980, 5U01DK060963, and 5U01DK060902). In addition, this work was supported in part by the following institutional Clinical Translational Science Awards and other NIH grants: University of Pennsylvania, UL1 RR024134; Johns Hopkins University, UL1 RR025005; University of Maryland, GCRC M01 RR16500; Case Western Reserve University Clinical and Translational Science Collaborative (University Hospitals of Cleveland, Cleveland Clinic Foundation, and MetroHealth), UL1 RR024989; University of Michigan, GCRC M01 RR-000042 and UL1 RR024986; University of Illinois at Chicago, UL1 RR029879; Tulane/LSU/Charity Hospital General Clinical Research Center, RR05096; and Kaiser-UCSF-CTSI, RR024131.

Received for publication December 16, 2010, and accepted in revised form August 25, 2011.

Address correspondence to: Myles Wolf, 1120 NW 14th Street, Suite 819, Miami, Florida 33136, USA. Phone: 305.243.7760; Fax: 305.243.8914; E-mail: mwolf2@med.miami.edu. Or to: Christian Faul, 1580 NW 10th Avenue, Batchelor Bldg. 626, Miami, Florida 33136, USA. Phone: 305.243.3206; Fax: 305.243.3209; E-mail: cfaul@med.miami.edu.

1. Coresh J, et al. Prevalence of chronic kidney disease in the United States. *JAMA*. 2007;298(17):2038–2047.
2. Go AS, Chertow GM, Fan D, McCulloch CE, Hsu CY. Chronic kidney disease and the risks of death, cardiovascular events, and hospitalization. *N Engl J Med*. 2004;351(13):1296–1305.
3. Zoccali C, et al. Prognostic value of echocardiographic indicators of left ventricular systolic function in asymptomatic dialysis patients. *J Am Soc Nephrol*. 2004;15(4):1029–1037.
4. Levy D, Garrison RJ, Savage DD, Kannel WB, Castelli WP. Prognostic implications of echocardiographically determined left ventricular mass in the Framingham Heart Study. *N Engl J Med*. 1990; 322(22):1561–1566.
5. Foley RN, et al. Clinical and echocardiographic disease in patients starting end-stage renal disease therapy. *Kidney Int*. 1995;47(1):186–192.
6. London GM, et al. Alterations of left ventricular hypertrophy in and survival of patients receiving hemodialysis: follow-up of an interventional study. *J Am Soc Nephrol*. 2001;12(12):2759–2767.
7. Paoletti E, Bellino D, Cassottana P, Rolla D, Cannella G. Left ventricular hypertrophy in nondiabetic predialysis CKD. *Am J Kidney Dis*. 2005;46(2):320–327.
8. Middleton RJ, Parfrey PS, Foley RN. Left ventricular hypertrophy in the renal patient. *J Am Soc Nephrol*. 2001;12(5):1079–1084.
9. Parfrey PS, et al. Impact of renal transplantation on uremic cardiomyopathy. *Transplantation*. 1995; 60(9):908–914.
10. Eswarakumar VP, Lax I, Schlessinger J. Cellular signaling by fibroblast growth factor receptors. *Cytokine Growth Factor Rev*. 2005;16(2):139–149.
11. Ornitz DM, Itoh N. Fibroblast growth factors. *Genome Biol*. 2001;2(3):REVIEWS3005.
12. Detillieux KA, Sheikh F, Kardami E, Cattini PA. Biological activities of fibroblast growth factor-2 in the adult myocardium. *Cardiovasc Res*. 2003; 57(1):8–19.
13. Parker TG, Packer SE, Schneider MD. Peptide growth factors can provoke "fetal" contractile protein gene expression in rat cardiac myocytes. *J Clin Invest*. 1990;85(2):507–514.
14. Scheinowitz M, et al. Basic fibroblast growth factor induces myocardial hypertrophy following acute infarction in rats. *Exp Physiol*. 1998;83(5):585–593.
15. Corda S, et al. Trophic effect of human pericardial fluid on adult cardiac myocytes. Differential role of fibroblast growth factor-2 and factors related to ventricular hypertrophy. *Circ Res*. 1997;81(5):679–687.
16. Frey N, Olson EN. Cardiac hypertrophy: the good, the bad, and the ugly. *Annu Rev Physiol*. 2003;65:45–79.
17. Heineke J, Molkentin JD. Regulation of cardiac hypertrophy by intracellular signalling pathways. *Nat Rev Mol Cell Biol*. 2006;7(8):589–600.
18. Molkentin JD. Calcineurin-NFAT signaling regulates the cardiac hypertrophic response in coordination with the MAPKs. *Cardiovasc Res*. 2004; 63(3):467–475.
19. Muslin AJ. MAPK signalling in cardiovascular health and disease: molecular mechanisms and therapeutic targets. *Clin Sci (Lond)*. 2008; 115(7):203–218.
20. Vega RB, Bassel-Duby R, Olson EN. Control of cardiac growth and function by calcineurin signaling. *J Biol Chem*. 2003;278(39):36981–36984.
21. Dorn GW 2nd, Force T. Protein kinase cascades in the regulation of cardiac hypertrophy. *J Clin Invest*. 2005;115(3):527–537.
22. Shimada T, et al. Cloning and characterization of FGF23 as a causative factor of tumor-induced osteomalacia. *Proc Natl Acad Sci U S A*. 2001; 98(11):6500–6505.
23. Ornitz DM. FGFs, heparan sulfate and FGFRs: complex interactions essential for development. *Bioessays*. 2000;22(2):108–112.
24. Goetz R, et al. Molecular insights into the klotho-dependent, endocrine mode of action of fibroblast growth factor 19 subfamily members. *Mol Cell Biol*. 2007;27(9):3417–3428.
25. Urakawa I, et al. Klotho converts canonical FGF receptor into a specific receptor for FGF23. *Nature*. 2006; 444(7120):770–774.
26. Kurosu H, et al. Regulation of fibroblast growth factor-23 signaling by klotho. *J Biol Chem*. 2006; 281(10):6120–6123.
27. Ben-Dov IZ, et al. The parathyroid is a target organ for FGF23 in rats. *J Clin Invest*. 2007;117(12):4003–4008.
28. Wolf M. Forging forward with 10 burning questions on FGF23 in kidney disease. *J Am Soc Nephrol*. 2010;21(9):1427–1435.
29. Gutierrez O, et al. Fibroblast growth factor-23 mitigates hyperphosphatemia but accentuates calcitriol deficiency in chronic kidney disease. *J Am Soc Nephrol*. 2005;16(7):2205–2215.
30. Isakova T, et al. Fibroblast growth factor 23 is elevated before parathyroid hormone and phosphate in chronic kidney disease. *Kidney Int*. 2011; 79(12):1370–1378.
31. Shimada T, et al. Circulating fibroblast growth factor 23 in patients with end-stage renal disease treated by peritoneal dialysis is intact and biologically active. *J Clin Endocrinol Metab*. 2010;95(2):578–585.
32. Gutierrez OM, et al. Fibroblast growth factor 23 and mortality among patients undergoing hemodialysis. *N Engl J Med*. 2008;359(6):584–592.
33. Jean G, et al. High levels of serum fibroblast growth factor (FGF)-23 are associated with increased mortality in long haemodialysis patients. *Nephrol Dial Transplant*. 2009;24(9):2792–2796.
34. Parker BD, et al. The associations of fibroblast growth factor 23 and uncarboxylated matrix Gla protein with mortality in coronary artery disease: the Heart and Soul Study. *Ann Intern Med*. 2010; 152(10):640–648.
35. Isakova T, et al. Fibroblast growth factor 23 and risks of mortality and end-stage renal disease in patients with chronic kidney disease. *JAMA*. 2011; 305(23):2432–2439.
36. Gutierrez OM, et al. Fibroblast growth factor 23 and left ventricular hypertrophy in chronic kidney disease. *Circulation*. 2009;119(19):2545–2552.
37. Mirza MA, Larsson A, Melhus H, Lind L, Larsson TE. Serum intact FGF23 associate with left ventricular mass, hypertrophy and geometry in an elderly population. *Atherosclerosis*. 2009;207(2):546–551.
38. Kardami E, et al. Fibroblast growth factor 2 isoforms and cardiac hypertrophy. *Cardiovasc Res*. 2004; 63(3):458–466.
39. Kostin S, Hein S, Arnon E, Scholz D, Schaper J. The cytoskeleton and related proteins in the human failing heart. *Heart Fail Rev*. 2000;5(3):271–280.
40. Morkin E. Control of cardiac myosin heavy chain gene expression. *Microsc Res Tech*. 2000;50(6):522–531.
41. Izumo S, et al. Myosin heavy chain messenger RNA and protein isoform transitions during cardiac hypertrophy. Interaction between hemodynamic and thyroid hormone-induced signals. *J Clin Invest*. 1987;79(3):970–977.
42. Lompre AM, Schwartz K, d'Albis A, Lacombe G, Van Thiem N, Swynghedauw B. Myosin isoenzyme redistribution in chronic heart overload. *Nature*.

1979;282(5734):105–107.
43. Molkentin JD, et al. A calcineurin-dependent transcriptional pathway for cardiac hypertrophy. *Cell*. 1998;93(2):215–228.
44. Komuro I, Yazaki Y. Control of cardiac gene expression by mechanical stress. *Annu Rev Physiol*. 1993; 55:55–75.
45. Barger PM, Kelly DP. Fatty acid utilization in the hypertrophied and failing heart: molecular regulatory mechanisms. *Am J Med Sci*. 1993;318(1):36–42.
46. Rimbaud S, et al. Stimulus specific changes of energy metabolism in hypertrophied heart. *J Mol Cell Cardiol*. 2009;46(6):952–959.
47. Kuro-o M, et al. Mutation of the mouse klotho gene leads to a syndrome resembling ageing. *Nature*. 1997; 390(6655):45–51.
48. Jaye M, Schlessinger J, Dionne CA. Fibroblast growth factor receptor tyrosine kinases: molecular analysis and signal transduction. *Biochim Biophys Acta*. 1992;1135(2):185–199.
49. Zhang X, Ibrahimi OA, Olsen SK, Umemori H, Mohammadi M, Ornitz DM. Receptor specificity of the fibroblast growth factor family. The complete mammalian FGF family. *J Biol Chem*. 2006; 281(23):15694–15700.
50. Yu X, et al. Analysis of the biochemical mechanisms for the endocrine actions of fibroblast growth factor-23. *Endocrinology*. 2005;146(11):4647–4656.
51. Mohammadi M, et al. Crystal structure of an angiogenesis inhibitor bound to the FGF receptor tyrosine kinase domain. *EMBO J*. 1998;17(20):5896–5904.
52. Katz M, Amit I, Yarden Y. Regulation of MAPKs by growth factors and receptor tyrosine kinases. *Biochim Biophys Acta*. 2007;1773(8):1161–1176.
53. Sugden PH, Clerk A. "Stress-responsive" mitogen-activated protein kinases (c-Jun N-terminal kinases and p38 mitogen-activated protein kinases) in the myocardium. *Circ Res*. 1998;83(4):345–352.
54. Bueno OF, et al. The MEK1-ERK1/2 signaling pathway promotes compensated cardiac hypertrophy in transgenic mice. *EMBO J*. 2000;19(23):6341–6350.
55. Buitrago M, et al. The transcriptional repressor Nab1 is a specific regulator of pathological cardiac hypertrophy. *Nat Med*. 2005;11(8):837–844.
56. Bogoyevitch MA, et al. Endothelin-1 and fibroblast growth factors stimulate the mitogen-activated protein kinase signaling cascade in cardiac myocytes. The potential role of the cascade in the integration of two signaling pathways leading to myocyte hypertrophy. *J Biol Chem*. 1994;269(2):1110–1119.
57. Crabtree GR, Olson EN. NFAT signaling: choreographing the social lives of cells. *Cell*. 2002; 109 suppl:S67–S79.
58. Wilkins BJ, Molkentin JD. Calcium-calcineurin signaling in the regulation of cardiac hypertrophy. *Biochem Biophys Res Commun*. 2004;322(4):1178–1191.
59. Frey N, et al. Calsarcin-2 deficiency increases exercise capacity in mice through calcineurin/NFAT activation. *J Clin Invest*. 2008;118(11):3598–3608.
60. Shioi T, et al. The conserved phosphoinositide 3-kinase pathway determines heart size in mice. *EMBO J*. 2000;19(11):2537–2548.
61. Amado LC, et al. Cardiac repair with intramyocardial injection of allogeneic mesenchymal stem cells after myocardial infarction. *Proc Natl Acad Sci U S A*. 2005; 102(32):11474–11479.
62. Antos CL, et al. Activated glycogen synthase-3 beta suppresses cardiac hypertrophy in vivo. *Proc Natl Acad Sci U S A*. 2002;99(2):907–912.
63. Molkentin JD, Kalvakolanu DV, Markham BE. Transcription factor GATA-4 regulates cardiac muscle-specific expression of the alpha-myosin heavy-chain gene. *Mol Cell Biol*. 1994;14(7):4947–4957.
64. Yin FC, Spurgeon HA, Rakusan K, Weisfeldt ML, Lakatta EG. Use of tibial length to quantify cardiac hypertrophy: application in the aging rat. *Am J Physiol*. 1982;243(6):H941–H947.
65. Di Marco GS, et al. Cardioprotective effect of calcineurin inhibition in an animal model of renal disease. *Eur Heart J*. 2011;32(15):1935–1945.
66. Finch JL, et al. Effect of paricalcitol and cinacalcet on serum phosphate, FGF-23, and bone in rats with chronic kidney disease. *Am J Physiol Renal Physiol*. 2010;298(6):F1315–F1322.
67. Hu MC, et al. Klotho deficiency causes vascular calcification in chronic kidney disease. *J Am Soc Nephrol*. 2010;22(1):124–136.
68. Kurosu H, Kuro OM. The Klotho gene family as a regulator of endocrine fibroblast growth factors. *Mol Cell Endocrinol*. 2009;299(1):72–78.
69. Wang H, et al. Overexpression of fibroblast growth factor 23 suppresses osteoblast differentiation and matrix mineralization in vitro. *J Bone Miner Res*. 2008; 23(6):939–948.
70. Galitzer H, Ben-Dov IZ, Silver J, Naveh-Many T. Parathyroid cell resistance to fibroblast growth factor 23 in secondary hyperparathyroidism of chronic kidney disease. *Kidney Int*. 2010;77(3):211–218.
71. Hughes SE. Differential expression of the fibroblast growth factor receptor (FGFR) multigene family in normal human adult tissues. *J Histochem Cytochem*. 1997;45(7):1005–1019.
72. Harmer NJ, Pellegrini L, Chirgadze D, Fernandez-Recio J, Blundell TL. The crystal structure of fibroblast growth factor (FGF) 19 reveals novel features of the FGF family and offers a structural basis for its unusual receptor affinity. *Biochemistry*. 2004; 43(3):629–640.
73. Jonsson KB, et al. Fibroblast growth factor 23 in oncogenic osteomalacia and X-linked hypophosphatemia. *N Engl J Med*. 2003;348(17):1656–1663.
74. Nehgme R, Fahey JT, Smith C, Carpenter TO. Cardiovascular abnormalities in patients with X-linked hypophosphatemia. *J Clin Endocrinol Metab*. 1997; 82(8):2450–2454.
75. Fuller TJ, Nichols WW, Brenner BJ, Peterson JC. Reversible depression in myocardial performance in dogs with experimental phosphorus deficiency. *J Clin Invest*. 1978;62(6):1194–1200.
76. O'Connor LR, Wheeler WS, Bethune JE. Effect of hypophosphatemia on myocardial performance in man. *N Engl J Med*. 1977;297(17):901–903.
77. Zoccali C, et al. Prognostic impact of the indexation of left ventricular mass in patients undergoing dialysis. *J Am Soc Nephrol*. 2001;12(12):2768–2774.
78. Oliveira RB, et al. Early control of PTH and FGF23 in normophosphatemic CKD patients: a new target in CKD-MBD therapy? *Clin J Am Soc Nephrol*. 2010; 5(2):286–291.
79. Hasegawa H, et al. Direct evidence for a causative role of FGF23 in the abnormal renal phosphate handling and vitamin D metabolism in rats with early-stage chronic kidney disease. *Kidney Int*. 2010; 78(10):975–980.
80. Feldman HI, et al. The Chronic Renal Insufficiency Cohort (CRIC) Study: Design and Methods. *J Am Soc Nephrol*. 2003;14(7 suppl 2):S148–S153.
81. Lang RM, et al. Recommendations for chamber quantification: a report from the American Society of Echocardiography's Guidelines and Standards Committee and the Chamber Quantification Writing Group, developed in conjunction with the European Association of Echocardiography, a branch of the European Society of Cardiology. *J Am Soc Echocardiogr*. 2005;18(12):1440–1463.
82. Bai XY, Miao D, Goltzman D, Karaplis AC. The autosomal dominant hypophosphatemic rickets R176Q mutation in fibroblast growth factor 23 resists proteolytic cleavage and enhances in vivo biological potency. *J Biol Chem*. 2003;278(11):9843–9849.
83. Toraason M, Luken ME, Breitenstein M, Krueger JA, Biagini RE. Comparative toxicity of allylamine and acrolein in cultured myocytes and fibroblasts from neonatal rat heart. *Toxicology*. 1989;56(1):107–117.
84. Bishopric NH, Simpson PC, Ordahl CP. Induction of the skeletal alpha-actin gene in alpha 1-adrenoceptor-mediated hypertrophy of rat cardiac myocytes. *J Clin Invest*. 1987;80(4):1194–1199.
85. Faul C, Huttelmaier S, Oh J, Hachet V, Singer RH, Mundel P. Promotion of importin {alpha}-mediated nuclear import by the phosphorylation-dependent binding of cargo protein to 14-3-3. *J Cell Biol*. 2005; 169(3):415–424.
86. Faul C, Dhume A, Schecter AD, Mundel P. Protein Kinase A, Ca2+/Calmodulin-dependent kinase II, and calcineurin regulate the intracellular trafficking of myopodin between the z-disc and the nucleus of cardiac myocytes. *Mol Cell Biol*. 2007; 27(23):8215–8227.
87. Faul C, et al. The actin cytoskeleton of kidney podocytes is a direct target of the antiproteinuric effect of cyclosporine A. *Nat Med*. 2008;14(9):931–938.
88. Lincoln J, Kist R, Scherer G, Yutzey KE. Sox9 is required for precursor cell expansion and extracellular matrix organization during mouse heart valve development. *Dev Biol*. 2007;305(1):120–132.
89. Bader D, Masaki T, Fischman DA. Immunochemical analysis of myosin heavy chain during avian myogenesis in vivo and in vitro. *J Cell Biol*. 1982; 95(3):763–770.